2-D BED SEDIMENT TRANSPORT MODELING OF A REACH ON THE SAGAVANIRKTOK RIVER, ALASKA

By

Isaac A. Ladines, B.S.

A Thesis Submitted in Partial Fulfillment of the Requirements

for the Degree of

Master of Science

in

Civil Engineering

University of Alaska Fairbanks

May 2019

APPROVED:

Dr. Horacio Toniolo, Committee Chair
Dr. David Barnes, Committee Member
Dr. Bill Schnabel, Committee Member
Dr. Leroy Hulsey, Chair
Department of Civil and Environmental Engineering
Dr. Bill Schnabel, Dean
College of Engineering and Mines
Dr. Michael Castellini, *Dean of the Graduate School*

Abstract

Conducting a 2-D sediment transport modeling study on the Sagavanirktok River has offered great insight to bed sediment movement. During the summer of 2017, sediment excavation of two parallel trenches began in the Sagavanirktok River, in an effort to raise the road elevation of the Dalton Highway to remediate against future floods. To predict the time in which the trenches refill with upstream sediment a 2-D numerical model was used. Three scenarios: (1) a normal cumulative volumetric flow, (2) a max discharge event, and (3) a max cumulative volumetric flow, were coupled with three sediment transport equations: Parker, Wilcock-Crowe and Meyer Peter and Müller for a total of 9 simulations. Results indicated that scenario (1) predicted the longest time to fill, ranging from 1-6 years followed by scenario (2), an even shorter time, and scenario (3) showing sustained high flows have the capability to nearly refill the trenches in one year. Because the nature of this research is predictive, limitations exist as a function of assumptions made and the numerical model. Therefore, caution should be taken in analyzing the results. However, it is important to note that this is the first time estimates have been calculated for an extraction site to be refilled on the Sagavanirktok River. Such a model could be transformed into a tool to project filling of future material sites. Ultimately, this could expedite the permitting process, eliminating the need to move to a new site by returning to a site that has been refilled from upstream sediment.

Table of Contents

Abstract ii
Table of Contents iii
List of Figures iv
List of Tables vi
List of Appendices vi
Acknowledgements vii
Chapter 1 - Introduction 1
1.1 Objective 2
1.2 Outline 3
Chapter 2 - Methodology 5
2.1 Numerical Model: SRH-2D 5
2.2 SRH-2D: Hydrodynamic Equations 6
2.3 SRH-2D: Sediment Transport Equations 7
2.3.1 Parker Function 9
2.3.2 Wilcock-Crowe Function 10
2.3.3 Meyer-Peter and Müller Function 10
2.4 Hydrologic Modeling Parameters 11
2.5 Sedimentological Modeling Parameters 17
2.6 Hydrologic Scenarios Used 20
Chapter 3 - Results and Discussion 22
3.1 Hydrologic Results 22
3.2 Sediment Transport Results 24
3.3 Modeling Assumptions and Limitations 33
Chapter 4 - Conclusions and Future Work 36
4.1 Conclusions 36
4.2 Future Work 36
Chapter 5 - References 38

List of Figures

Figure 1: Sagavanirktok River near MP367 showing model domain and trench locations. Flow direction is from bottom to top. The polygon furthest left represents the west trench (1) and the polygon furthers right represents the east trench (2) 4
Figure 2: Model mesh showing terrain elevation measured in meters. Flow direction is from bottom to top 12
Figure 3: Oblique view of channels leading into the east and west trenches 13
Figure 4: Model domain showing boundary conditions of the inlet (blue) and outlet (red) 14
Figure 5: Hydrographs showing the variation in discharge between each of the model scenarios 15
Figure 6: Materials coverage denoting Manning's Roughness values for the model domain 16
Figure 7: Observed velocity cross section at the Sagavanirktok River below the Ivishak River confluence at DSS2 on June 24, 2016, at measured flows of ~ 500 m3/s. Measured velocities range from 0 (pink) to 3.8 m/s (red) 17
Figure 8: Sediment materials coverage denoting areas of active sediment transport 19
Figure 9: Model grain size distribution input 20
Figure 10: Scenario 2:(left) velocity magnitude (m/s) on day 69 (right) velocity magnitude (m/s) on day 71 during the peak event 23
Figure 11:Scenario 2:(left) water depth (m) on day 69 (right) water depth (m) on day 71 during the peak event 24
Figure 12: Deposited trench sediment in m^3 for east and west trench as compared to the scenario 1 hydrograph 25
Figure 13: Comparison of bed elevation in meters. Far left, (a) is the initial elevation. The three figures right show the simulation end for (b) Parker Eq. (c) W-C Eq. and (d) MPM Eq. 26
Figure 14: Time series of west trench comparing bed elevation for each sediment transport equation during scenario 1 27

Figure 15: Percent of west trench filled during scenario 1 28
Figure 16: Time series of east trench comparing bed elevation for each sediment transport equation during scenario 1 28
Figure 17:Percent of east trench filled during scenario 1 29
Figure 18: The percent of the west and east trench refilled for each scenario under each equation 31
Figure 19: The time in years to fill the west trench based on a linear approximation of scenario 1 results (* denotes that the original Meyer Peter Muller results were halved in accordance with Wong & Parker (2006)) 32
Figure 20:The time in years to fill the east trench based on a linear approximation of scenario 1 results(* denotes that the original Meyer Peter Muller results were halved in accordance with Wong & Parker (2006)) 32
Figure 21: East view of pit on October 25, 2018 Pit remnant is visible at left. Red curve indicates approximate edge of pit as surveyed in September. Numbers indicate sediment sampling locations (Toniolo et al., 2018) 33

Figure A.1: Oblique view of trenches drawn in AutoCAD 40
Figure A.2: Comparison of model domain with trenches and without trenches 41

Figure B.1: (a) preliminary mesh (b) 2nd mesh (c) 3rd mesh (d) final mesh 43
Figure B.2: Plan view of model domain showing arcs through the west trench and through the main channel 44
Figure B.3: West channel profile from Figure B.2 comparing the three preliminary meshes 45
Figure B.4: Main channel profile from Figure B.2 comparing the three preliminary meshes 45

Figure C.1: Transport equation coefficients for the Parker equation and non-transport equation dependents 47

Figure C.2: Transport equation coefficients for the W-C equation and non-transport equation dependents 47
Figure C.3:Transport equation coefficients for the MPM equation and non-transport equation dependents 48

Figure D.1: Deposited trench sediment in m^3 for east and west trench as compared to the scenario 2 hydrograph 49
Figure D.2:Comparison of bed elevation in meters. Far left, (a) is the initial elevation. The three figures right show the simulation end for (b) Parker Eq. (c) W-C Eq. and (d) MPM Eq. 49
Figure D.3: Time series of west trench comparing bed elevation for each sediment transport equation during scenario 2 50
Figure D.4: Percent of west trench filled during scenario 2 50
Figure D.5: Time series of east trench comparing bed elevation for each sediment transport equation during scenario 2 51
Figure D.6: Percent of east trench filled during scenario 2 51

List of Tables

Table 1: Volume of sediment measured for each scenario under each equation 29

List of Appendices

Appendix A Trench Creation 40
Appendix B Model Mesh Evolution and Configuration 42
Appendix C Sediment Transport Equation Parameters 46
Appendix D Scenario 2 49
Appendix E Scenario 3 52

Acknowledgements

I would like to express my greatest gratitude to Dr. Horacio Toniolo, who I am happy to call both a mentor and a friend. He offered me a wonderful opportunity to understand the importance of research in the engineering world and introduced me to the fascinating complexity of sediment transport. Secondly, I would like to thank Scott Hogan for providing answers to many questions I had throughout the modeling process. More importantly, I am especially grateful he provided me the software to make this research a reality.

I would like to thank my committee members Dr. Dave Barnes and Dr. Bill Schnabel for being a part of my committee and providing key feedback during my research. I thank Melanie Engram, who greatly helped with guiding me through ArcGIS, and Emily Youcha, for assisting me through the development of key figures in this research.

I would also like to thank my fellow graduate students, namely Kelsey Dean, Eric LaMesjerant and Jenah Laurio who are great friends that, despite having their own busy schedule, were always able to provide advice and direction during my grad school experience.

I would also like to thank my family for listening to my long rants about the errors I struggled to resolve for my modeling. They were able to help me see the bigger picture and the problems would seemingly solve themselves in the following days.

Last but not least, I would like to thank my future wife, Cassi Williams, for the constant love and support she provided me during my entire grad school studies, without which, would have been of the utmost difficulty.

Chapter 1 - Introduction

Overwinter conditions in Arctic rivers are key for the survival of fish living in those aquatic environments. Subsequently, manmade depressions in the river, such as gravel extraction for road construction purposes, could provide a sustainable overwinter habitat. However, as the time passes, one could expect that the trenches made in the river will refill due to the natural bed load transport process of the river. The use of a numerical model could help to provide insight on the time needed for the river to refill a given material site. In the case of the Sagavanirktok (Sag) River, the time of refill is unknown, and so applying a numerical model, this research looks to address this problem.

The Sag River resides in the North Slope Borough of Alaska extending roughly 180 miles from the north slope of the Brooks Range and then flowing into the Beaufort Sea just east of Prudhoe Bay. The Sag river basin drains approximately 13, 500 km^2 of the Brooks range and North Slope (Toniolo et al., 2018). Characterized by extensive braiding and occasional bars with shrubs, its width varies from narrow to a few miles wide (Toniolo et al., 2017b). It is fed by a combination of snowmelt, rain and summer glacier melt (Toniolo et al., 2018).

Paralleling the Sag River is the Dalton Highway. Because it is the sole route for ground transportation from Fairbanks to Prudhoe Bay, it is a significant corridor for transporting supplies for the oil and gas industry. In the early part of 2015, major flooding from the Sag washed out sections of the Dalton Highway. The road damage was extensive and the highway was shut down to traffic for a three week span (Toniolo et al., 2017a). As a result of the substantial road damage during the flooding, an effort has been put forth to bring the road surface above the flood plain to remediate against further inundation events. To increase the height of the road, aggregate was pulled from the Sag in the form of two parallel trenches (cells) by Alaska Department of Transportation and Public Facilities (ADOT&PF) and their contractor, Cruz Construction. The extraction site for the project resides between MP366 and MP367 of the Dalton Highway.

Riverine gravel extraction has long been a source for concrete aggregate and other construction purposes. Throughout most of the Western United States the mining of fluvial gravels is quite common (Parker, 2008). Without proper guidelines, the impact from mining activities can lead to acute bed degradation downstream resulting in bridge failures and exposure of buried pipelines (Galay, 1983). While the Sag river flows through mostly remote locations with only one bridge, the Trans-Alaska Pipeline System parallels the river on many occasions. Therefore, it is paramount to ensure gravel

mining operations do not alter the river configuration in a way that would jeopardize its infrastructure.

Although ensuring the stability of manmade structures on the river is first and foremost, there are signs that indicate that gravel extraction on the North Slope has been shown to provide benefits for local fish populations. Past field investigations corroborate that known over wintering habitats for fish populations in the lower Sag and Kuparuk rivers are limited to several deep isolated pools during winter ice coverage (McLean, 1993). By extracting sediment from the river, it can provide effective wintering grounds for fish populations. In this way, the guideline set by Alaska Department of Fish and Game, outlined by McLean (1993), strikes a balance between enhancing fish and wildlife while simultaneously meeting the industry needs for gravel and water.

Shown in Figure 1 are the estimated positions of the trenches where aggregate was to be extracted. The mining and reclamation plan, supplied by ADOT&PF, estimate trench one and two to be 2800ft (853m) and 3100ft (945m) in length respectively. Both have a width of 300ft (91m) with a target depth of 20ft (6m). The two trenches conform to a trapezoidal shape with inside slopes of 3H:1V and outside slopes of 4H:1V. Slopes for the upstream and downstream portions of the cells are not to exceed 6H:1V.

A research team from the University of Alaska Fairbanks (UAF) collected topo-bathymetric data, between MP366 and MP367 of the Dalton Highway, acknowledging the proposed trench excavation sites (Toniolo et al., 2017b). With the union of the topographic and bathymetric data sets a digital elevation model (DEM) was created of the local river reach.

While the guideline prepared by McLean (1993) excellently describes the importance of site selection and general performance and reclamation guidelines, it does not mention how such extraction sites may refill over time with upstream sediment. Additionally, this may impact the fish populations, previously using the area for over wintering. Therefore, the work presented here, which is related to sedimentation processes in manmade sites in the river, provides relevance to this topic and aims to answer the question of how long it may take a material site to fully refill.

1.1 Objective

The main objective of this research was to estimate the time the trenches will refill under three different input scenarios: (1) a normal cumulative volumetric flow, (2) a max discharge event and (3) a max cumulative volumetric flow, utilizing three sediment transport equations for each scenario. In order to accomplish this, a hydro-sedimentological model was implemented.

1.2 Outline

Presented in Chapter 2 are the model, model equations, and the model input parameters used to approach this research. Hydrologic and sedimentological results and model assumptions and limitations are presented in Chapter 3. Conclusions and thoughts on applications for future work are shown in Chapter 4. Appendices disclose additional steps used to create the model and additional results obtained from the model. Specifically, Appendix A follows the methods used to create the trenches followed by restructuring the DEM by replacing the original survey data with the location of the proposed trenches. Appendix B shows the evolution of the mesh generation. Appendix C outlines specific details of sediment transport equation coefficients and additional non-dependent parameters. Appendix D and E shows the results from scenarios 2 and 3 respectively.

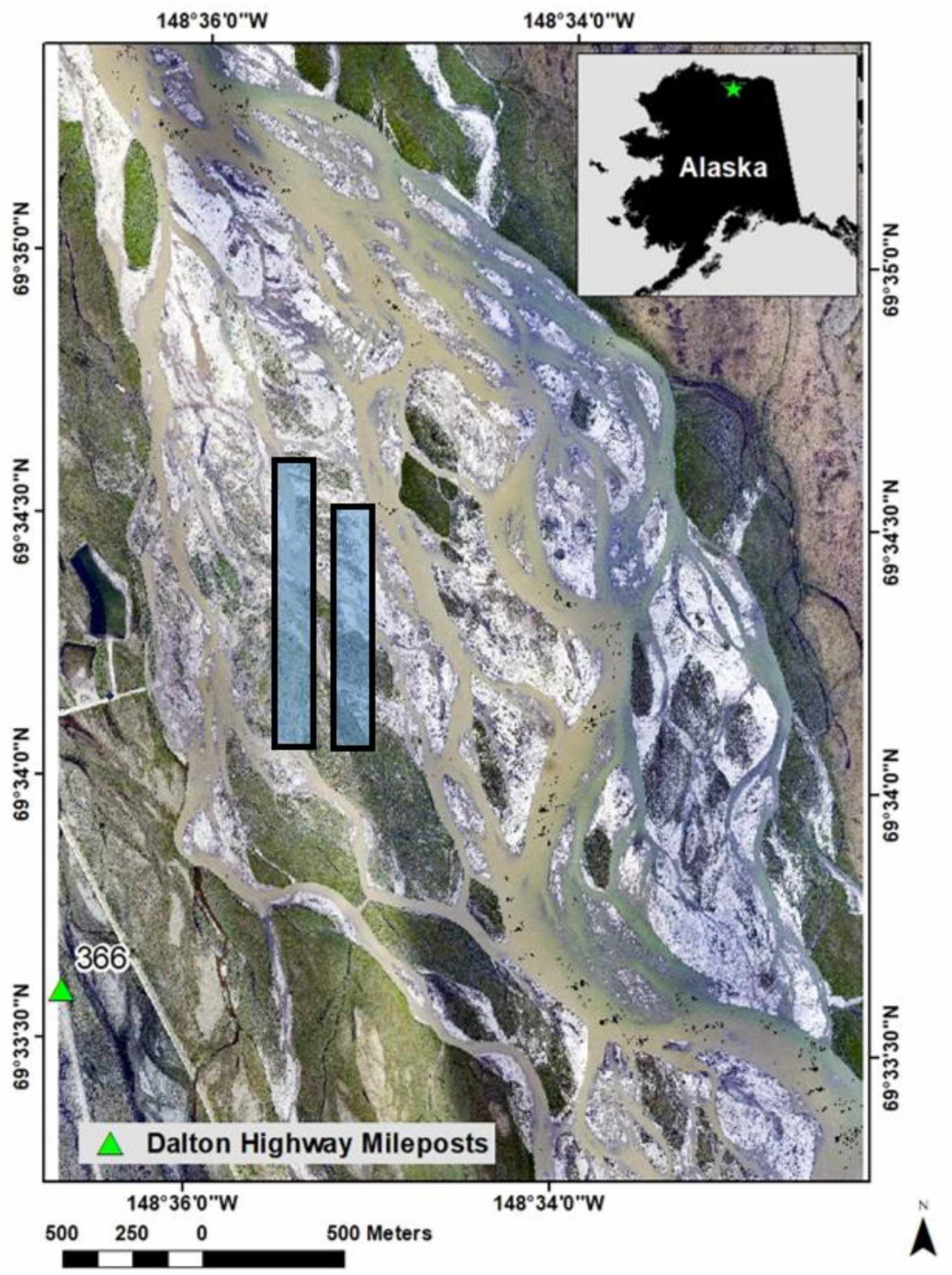

Figure 1: Sagavanirktok River near MP367 showing model domain and trench locations. Flow direction is from bottom to top. The polygon furthest left represents the west trench (1) and the polygon furthers right represents the east trench (2)

Chapter 2 - Methodology

Included below are the description of the chosen numerical model, the associated hydrodynamic and sedimentological equations in the model and a brief description of the sediment transport equations used in the simulations.

2.1 Numerical Model: SRH-2D

The Sedimentation and River Hydraulics-Two-Dimensional model (SRH-2D) is a 2D hydraulic numerical model based on 2D hydraulic principles and considerations for sediment transport, temperature and vegetation. It has been in development since 2004 by Dr. Yong Lai at the US Bureau of Reclamation.

SRH-2D solves the St Venant equations (2D depth averaged) using a finite-volume method. From the time of its creation it has been successfully used and tested for a number of scenarios (e.g. Lai, 2008, 2010).

SRH-2D has been developed with the thought to ensure a quality and efficient running 2-D model while limiting the complexity of its use. To conduct a full analysis using SRH-2D, it requires a third party software to perform pre and post processing elements. Developed by Aquaveo, the Surface-water Modeling System (SMS) fulfills this role as the graphical user interface for this work. SMS streamlines the model efficiency reducing the amount of commands needed for the creation of a model. In this way, many user errors can be identified and removed before moving forward with the final analysis (Lai, 2008).

There are two main modules used by SRH-2D including the FLOW module and MOBILE module. The FLOW module is utilized solely for hydrologic simulations while the MOBILE module considers both hydrologic and sedimentological simulations, the emphasis for this study.

SRH-2D is a robust 2D model, exceptionally useful for this project because of its ability to vividly recreate complex braided river systems within the model domain. In this way, morphological changes can be more easily observed.

2.2 SRH-2D: Hydrodynamic Equations

The following description of the numerical approach used in SRH-2D follows the work conducted by Lai (2008).

Because most open channels are shallow, the vertical motion component within the reach is negligible. With this knowledge, the three-dimensional Navier-Stokes equations can be averaged vertically to arrive at a series of depth averaged two-dimensional equations better known known as the 2D St. Venant equations:

$$\frac{\partial \mathrm{h}}{\partial \mathrm{t}} + \frac{\partial \mathrm{hU}}{\partial \mathrm{x}} + \frac{\partial \mathrm{hU}}{\partial \mathrm{y}} = e \tag{1}$$

$$\frac{\partial \mathrm{hU}}{\partial \mathrm{t}} + \frac{\partial \mathrm{hUU}}{\partial \mathrm{x}} + \frac{\partial \mathrm{hVU}}{\partial \mathrm{y}} = \frac{\partial \mathrm{h}T_{xx}}{\partial \mathrm{x}} + \frac{\partial \mathrm{h}T_{xy}}{\partial \mathrm{y}} - gh\frac{\partial \mathrm{z}}{\partial \mathrm{x}} - \frac{\tau_{bx}}{\rho} + D_{xx} + D_{xy} \tag{2}$$

$$\frac{\partial \mathrm{hV}}{\partial \mathrm{t}} + \frac{\partial \mathrm{hUV}}{\partial \mathrm{x}} + \frac{\partial \mathrm{hVV}}{\partial \mathrm{y}} = \frac{\partial \mathrm{h}T_{xy}}{\partial \mathrm{x}} + \frac{\partial \mathrm{h}T_{yy}}{\partial \mathrm{y}} - gh\frac{\partial \mathrm{z}}{\partial \mathrm{y}} - \frac{\tau_{by}}{\rho} + D_{yx} + D_{yy} \tag{3}$$

Where t is time, x and y are horizontal Cartesian coordinates, h is water depth, U and V are depth-averaged velocity components in the x and y respectively, e is excess rainfall rate, and g is the force of gravity. The depth averaged turbulent stresses, T_{xx}, T_{yy}, and T_{xy}, utilize the Boussinesq approach as:

$$T_{xx} = 2(\nu + \nu_t)\frac{\partial \mathrm{U}}{\partial \mathrm{x}} - \frac{2}{3}k \tag{4}$$

$$T_{yy} = 2(\nu + \nu_t)\frac{\partial \mathrm{V}}{\partial \mathrm{y}} - \frac{2}{3}k \tag{5}$$

$$T_{xy} = 2(\nu + \nu_t)\left(\frac{\partial \mathrm{V}}{\partial \mathrm{y}} + \frac{\partial \mathrm{V}}{\partial \mathrm{x}}\right) \tag{6}$$

Where ν is kinematic viscosity and ν_t is eddy viscosity and k is the turbulent kinetic energy. The eddy viscosity is calculated using a turbulence model. Two turbulence models, discussed by Rodi (1993), are utilized in SRH-2D: The k-ε model and the parabolic model. Choosing the parabolic model as the sole

turbulence model for this project, the eddy viscosity is calculated as:

$$\nu_t = C_t U_* h \tag{7}$$

U_* is the frictional velocity described below and C_t is the model constant ranging from 0.3 to 1.0. For this study, the default value of 0.7 is used. The bed friction is calculated by applying Manning's roughness equation:

$$\begin{pmatrix}\tau_{bx}\\ \tau_{by}\end{pmatrix} = \rho U_*^2 \frac{\binom{U}{V}}{\sqrt{U^2+V^2}} = \rho C_f \sqrt{U^2+V^2}\begin{pmatrix}U\\ V\end{pmatrix};\ C_f = \frac{gn^2}{h^{1/3}} \tag{8}$$

Where n is Manning's roughness coefficient.

Considering the governing equations discussed, they can be discretized using a finite volume numerical method, following the work done by Lai (1997, 2000) and Lai, Weber, & Patel (2003). The solution domain is wrapped by an unstructured mesh, typically composed of triangular and quadrilateral elements. The use of an unstructured mesh permits complex topographic and bathymetric features within a domain to be more accurately depicted. At the center of each element, the dependent variables (i.e. water level and bed elevation) are stored while velocities are calculated at each element face.

2.3 SRH-2D: Sediment Transport Equations

The description of SRH-2D sediment transport follows the work of Lai, Holburn, & Bauer (2006) demonstrated in a previous model (GSTAR-W). Over time, GSTAR-W evolved into SRH-2D, using the same suite of equations.

The SRH-2D internal sediment module represents the chosen sediment transport model. The model has a range of sediment transport equations, three of which pertain to bed load transport. Analysis of sediment assumed a fixed bed elevation, non-uniform sediment, and non-cohesive sediment. SRH-2D assumes sediment transport takes place in a way such that the bed elevation is a function of time, necessitating another equation to follow its evolution. This equation follows that rate of change in bed level is equal to the variance of the sediment flux, loosely described as sediment continuity. Such variation can be quantified by several sediment transport formulas.

The Sediments are divided into a number of sediment size classes. Each size class (k) follows the

relationship for mass conservation providing non-equilibrium transport expressed as:

$$\frac{\partial \mathrm{h}C_k}{\partial \mathrm{t}} + \frac{\partial \mathrm{hU}C_k}{\partial \mathrm{x}} + \frac{\partial \mathrm{hV}C_k}{\partial \mathrm{y}} = \frac{1}{L_b}(q_k^* - \sqrt{U^2 + V^2}hC_k) \tag{9}$$

where h is water depth; t is time; C_k is depth-averaged sediment concentration by volume for k_{th} sediment size class; U and V are depth-averaged velocity components respectively in x and y direction; L_b is the non-equilibrium adaptation length and q_k^* is the fractional sediment transport capacity for the k_{th} size class.

To account for changes in bed elevation, the bed sediment dynamics and interactions with the bed material load transport were simulated. Change in bed elevation (z_b) from the sediment size class k can then be calculated as:

$$(1 - p_b)\left(\frac{\partial z_b}{\partial \mathrm{t}}\right)_k = -\frac{1}{L_b}(q_k^* - \sqrt{U^2 + V^2}hC_k) \tag{10}$$

where p_b is the bed material porosity. For this research, the fixed bed approach was followed, where the sediment dynamics were a function of equation (10). This includes the deposition and erosion rates, changes in bed gradation and the sediment transport rate. The fixed bed approach is appropriate for this research because it sufficiently captures the sediment deposition for each trench.

Because we are only interested in bed load, the term $C_k = 0$. This simplifies the left hand side of Eq. 9 down to zero. Eq. (9) and Eq. (10) can then be linked to solely investigate bed load transport.

For the purpose of this work, three equations were selected to estimate the bed sediment transport:

- Parker (1990),
- Wilcock-Crowe (2003), and
- Meyer Peter and Müller (1948).

Two of them, Parker and Wilcock-Crowe are capable of handling multiple grain sizes, while Meyer-Peter and Müller considers a single grainsize.

In SRH-2D there are two distinct layers that constitute the sediment domain:

- Active Layer, and
- Subsurface layer(s).

At the surface, the active layer participates in the sediment exchange between the bed and bed load. The subsurface layer provides the sediment supply to the active layer once fully eroded. The active layer gradation equation is presented as:

$$\frac{\partial \delta_a p_{ak}}{\partial t} = (\frac{\partial z_b}{\partial t})_k + p^*_{ak}(\frac{\partial \delta_a}{\partial t} - \frac{\partial z_b}{\partial t}) \quad (11)$$

Where δ_a is the layer thickness of the active layer; p_{ak} is the active layer volumetric fraction of sediment size class k ;$(\sum_k p_{ak} = 1)$

$$p^*_{ak} = P_{ak} \quad if \ldots \left(\frac{\partial \delta_a}{\partial t} - \frac{\partial z_b}{\partial t}\right) < 0; \quad (12)$$

P_{ak} = sub-surface fraction of sediment size class k $if \ldots \left(\frac{\partial \delta_a}{\partial t} - \frac{\partial z_b}{\partial t}\right) < 0$; and

$$\frac{\partial z_b}{\partial t} = \sum_k (\frac{\partial z_b}{\partial t})_k \quad (13)$$

The sediment transport rate changes as a result of changes within the gradation of the active layer.

2.3.1 Parker Function

The Parker (1990) sediment transport equation has been shown to work most effectively in gravel rivers, which makes it a good fit for the Sag River. From collected field data, Parker (1990) developed the following formula:

$$\frac{q_{sk} g(s-1)}{(\frac{\tau_b}{\rho})^{1.5}} = p_k G(\varphi_k) \qquad and \qquad \varphi_k = \frac{\theta_k}{\theta_c}\left(\frac{d_k}{d_{50}}\right)^{\alpha}(1-p_b)\left(\frac{\partial z_b}{\partial t}\right)_k \quad (14)$$

A few variables within the primary equation are further described by the following set of equations:

$$q^*_k = \frac{q_{sk}}{q} \quad (15)$$

$$s = \frac{\rho_s}{\rho - 1} \quad (16)$$

$$\theta_k = \tau_b/[\rho g(s-1)d_k] \tag{17}$$

where q_{sk} is the volumetric sediment transport rate per unit width, p_k is the volumetric fraction of the k^{th} sediment size class in the bed, ρ and ρ_s are the water and sediment density respectively, τ_b is the bed shear stress θ_k is the Shield's parameter of sediment size class k, θ_c,is critical Shield's parameter, set at 0.045, d_k is diameter of sedimnet size class k and d_{50} is the median diameter of sediment mixture in the bed. $G(\varphi_k)$ relates to the field data that is further explained in Parker (1990).

2.3.2 Wilcock-Crowe Function

Following a similar approach to Parker (1990),in the form of a bed load formula, Wilcock & Crowe (2003) write their expression as:

$$W_i^* = f(\frac{\tau}{\tau_{ri}}) \tag{18}$$

where τ = bed shear stress, τ_{ri} = reference value of τ and W_i^* is equal to the following equation

$$W_i^* = \frac{(s-1)gq_{bi}}{F_i u_*^3} \tag{19}$$

where the values were similarly defined in the Parker equation with the exception that F_i is the proportion of size i on the bed surface and u_* = the shear velocity.

The critical Shields parameter (τ_c^*) for the Wilcock-Crowe (W-C) equation is set as 0.03, important for later discussion in this paper. Further details regarding the development of this equation are located in Wilcock & Crowe (2003).

2.3.3 Meyer-Peter and Müller Function

Meyer-Peter and Müller (MPM) (1948) developed a formula that is arguably the most well-known transport formula for gravel or coarse sediment. The original formula can be expressed as follows:

$$q_k^* = 8(\tau^* - \tau_c^*)^{3/2} \tag{20}$$

Where τ^* is the Shields parameter and $\tau_c^* = 0.047$ is defined as the critical Shields parameter.

Dissimilar to both the Parker and the W-C equation, the MPM equation uses only one grain size to predict sediment transport.

While a correction exists that accounts for the unnecessary energy slope correction in this formula, it was not integrated into this numerical model, suggesting that outputs from the Meyer-Peter and Muller equation should be considered with caution. Developed by Wong & Parker (2006), their reanalysis indicated that the original MPM equation values nearly doubled the actual sediment transport. Further discussions regarding this point are shown in Chapter 3.

2.4 Hydrologic Modeling Parameters

Before carrying out any sediment transport simulations a series of hydraulic simulations were run to ensure model stability and accuracy. However, before any simulations are conducted, the terrain data must first be introduced for the basis of the model.

The elevation input data used for the basis of this hydraulic model are a composition of UAF and Cruz Construction bathymetric survey data and a Structure from Motion (SfM) digital elevation model of the surrounding topography. The 0.2 m digital elevation model was resampled to 10 m x 10 m raster pixel size to improve the efficiency of preprocessing tasks. The raster elevation data were converted to scatter elevation data (x, y, z coordinate data). However, because the surveys and digital elevation model were created prior to the excavation of the trenches, additional steps were needed to replace the original topography with the projected trench locations and the paths leading into and out of the trenches. Specifics regarding this procedure are located in Appendix A.

For a hydraulic model to be carried out using SRH-2D, four important steps must be taken using SMS:

- Create Mesh,
- Define boundary conditions,
- Identify material input parameters, and
- Establish monitor points.

The model domain was created by drawing a perimeter around the scatter data. The perimeter arc vertices were then distributed and a polygon was created consisting of each of the arcs drawn to encompass the domain. Following this step, the scatter elevation dataset was set as the bathymetry

source for the creation of a mesh. A number of meshes were created to strike a balance between accuracy of the river reach and computation efficiency. The procedure outlining the mesh evolution can be found in Appendix B. The following mesh (Figure 2) represents the final iteration that is wrapped around the provided digital elevation model. Figure 3 shows an oblique view of the trenches providing a better angle of the area with the highest concentration of elements. In total, the number of elements used for this model was 19,269.

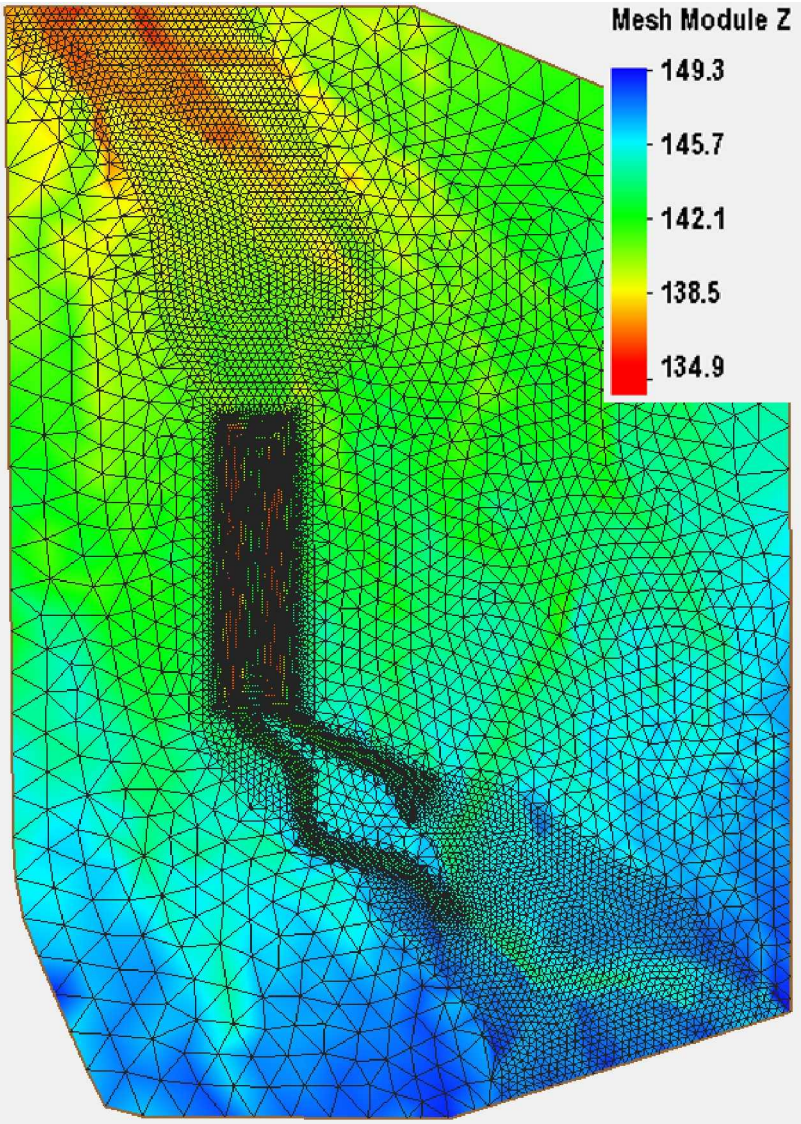

Figure 2: Model mesh showing terrain elevation measured in meters. Flow direction is from bottom to top

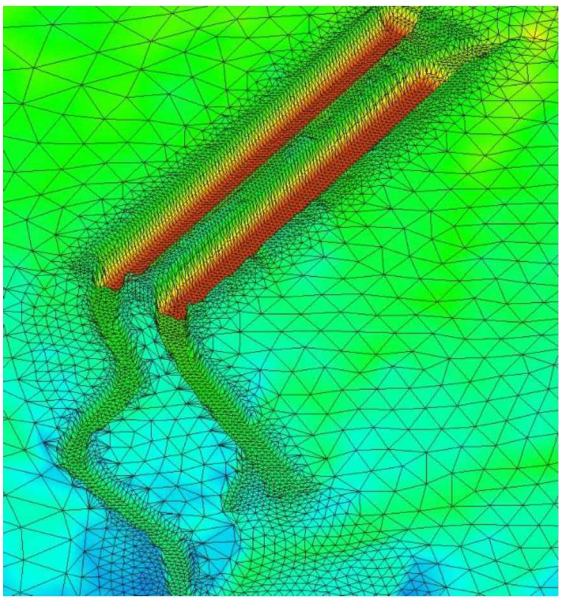

Figure 3: Oblique view of channels leading into the east and west trenches

In the next step, the boundary conditions were established. The inflow and outflow arcs are defined where an arc symbolizes an opening in the mesh from which water can enter and exit (Figure 4). There are three respective hydrographs utilized for this research (Figure 5). Scenario 1 was recorded during 1997. This hydrograph was chosen on the premise that it best represented a typical cumulative volumetric flow that would be seen on the Sag River during the summer months. Two additional hydrographs were chosen to represent more extreme events, one from 2002 and the other from 2018. The hydrograph from the summer of 2002, accounts for the greatest singular discharge event on record. At its peak, discharge built up to and exceeded 2700 m^3/s in the course of a few days. The hydrograph from the summer of 2018 demonstrated the largest cumulative volumetric quantity of discharge over the span of one summer. Because the location of the USGS station used to record these discharges is upstream of the confluence of the Sag River and the Ivishak River, the discharge for all three hydrographs was multiplied by two. Knowing both rivers have similar drainage basin sizes, the justification for such an assumption can be made to better predict the discharge expected through the modeled river reach.

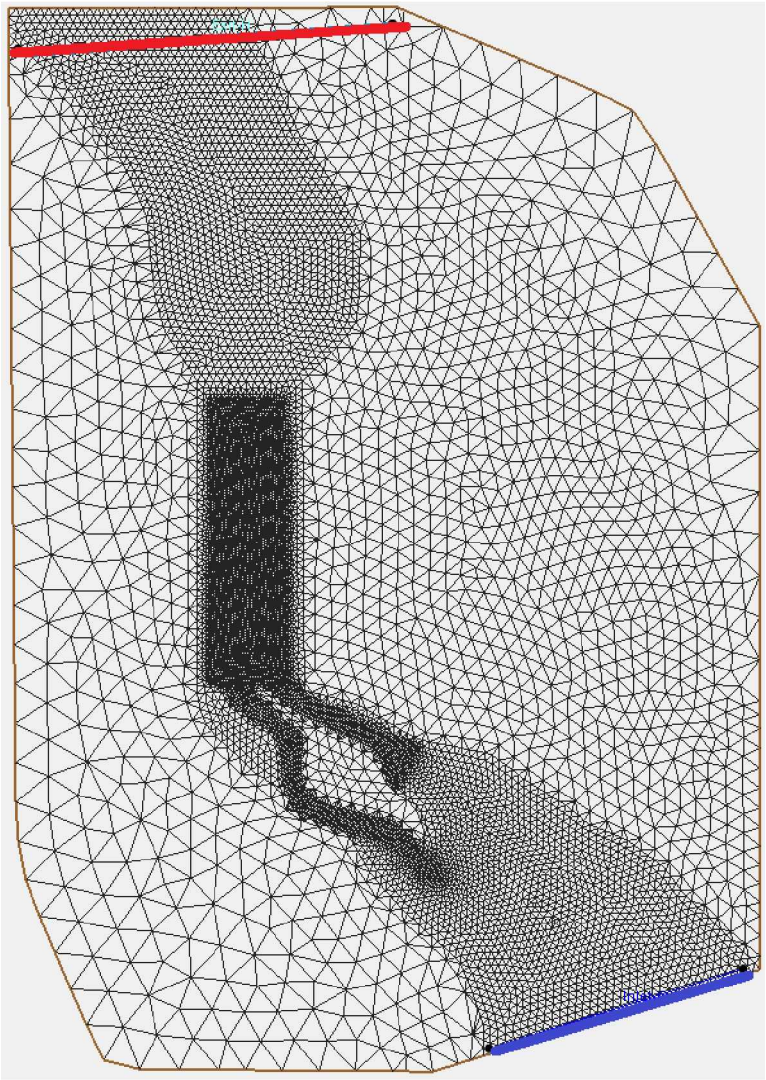

Figure 4: Model domain showing boundary conditions of the inlet (blue) and outlet (red)

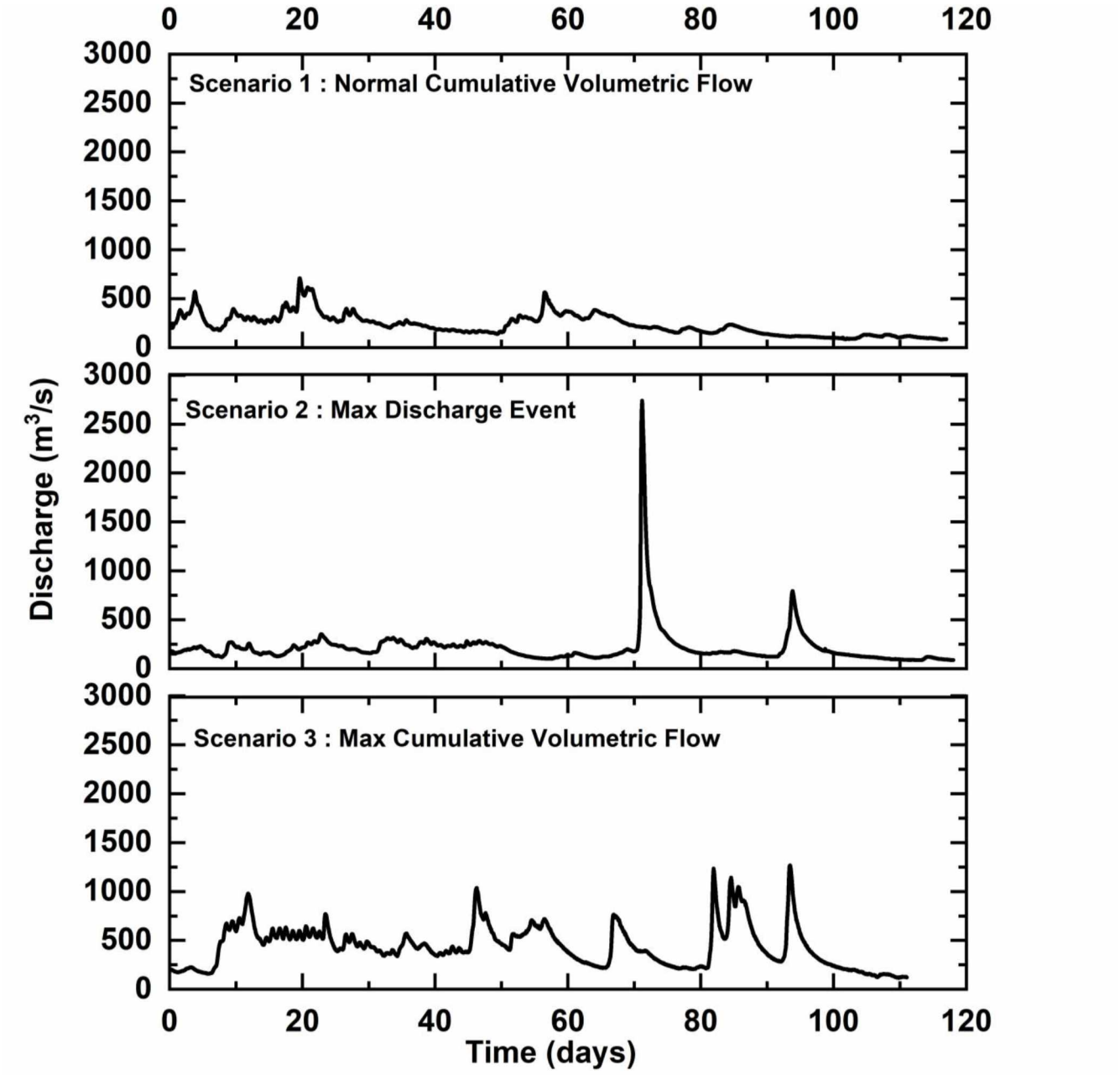

Figure 5: Hydrographs showing the variation in discharge between each of the model scenarios

The input parameter, the hydraulic roughness (or Manning's n), for the materials were then defined. The model domain was classified as two distinct materials: 1) active river channels and 2) the surrounding sand/gravel bars and vegetation. The river channels were given a Manning's n of 0.035 to denote a, lower stage winding channel with some deep pools and stones. Materials outside the main channel including the sand bars, gravel bars, and vegetation, were assigned a single Manning's n of

0.040. Both coefficients were obtained from Chow (1959). The classifications of each material are shown in Figure 6.

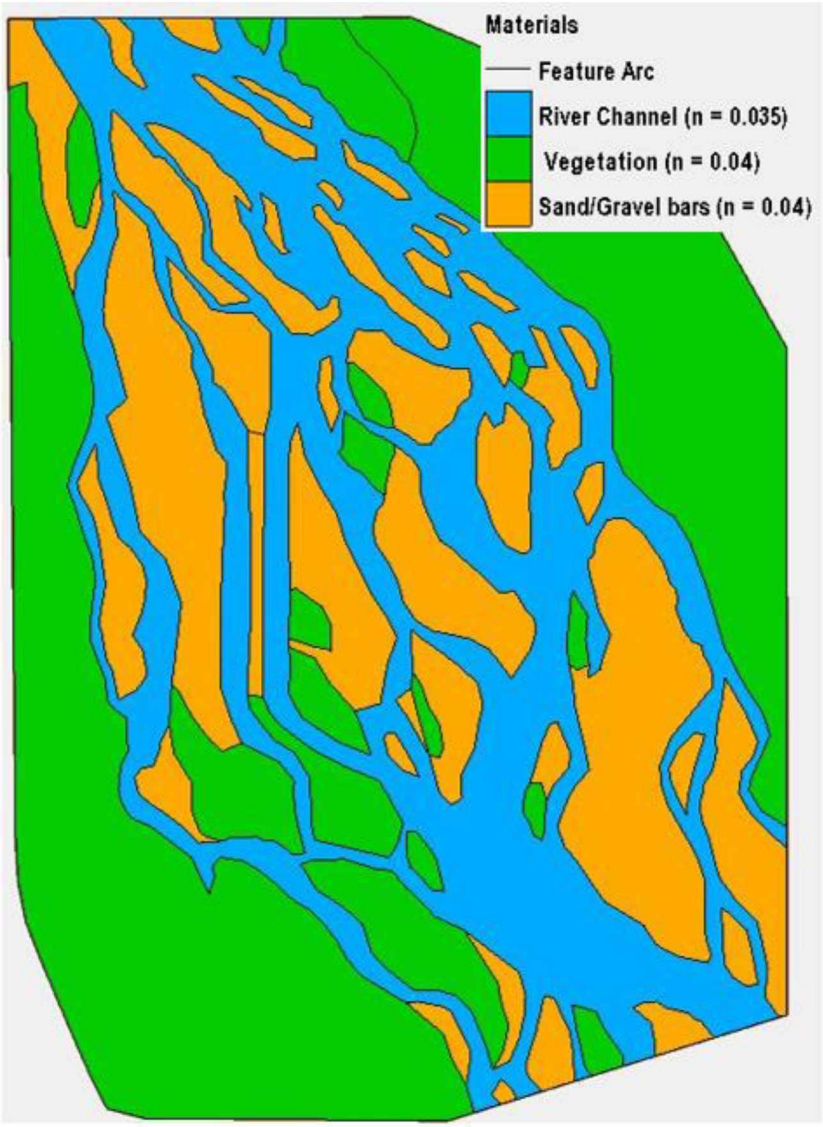

Figure 6: Materials coverage denoting Manning's Roughness values for the model domain

Figure 6 shows the final Manning's values for the entire domain. Several trials were conducted, during the Manning's n calibration process, to obtain similar velocity results as the one provided in Figure 7, which represents a velocity profile measured in the vicinity of the studied area. Additional details are available in Toniolo et al., (2017b).

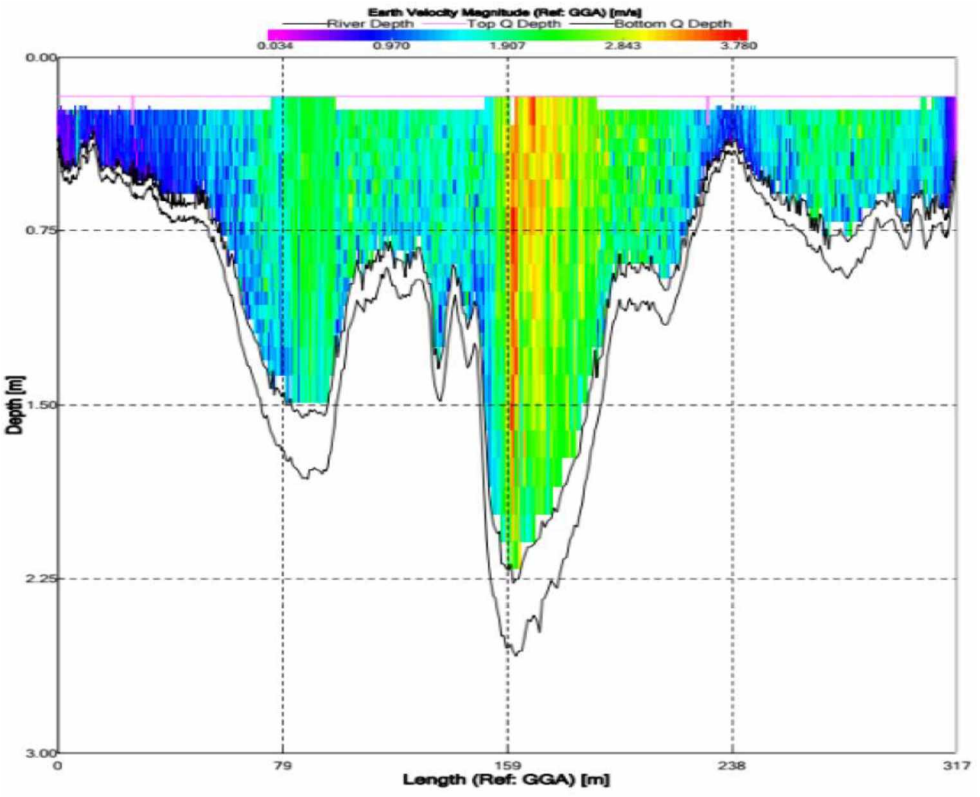

Figure 7: Observed velocity cross section at the Sagavanirktok River below the Ivishak River confluence at DSS2 on June 24, 2016, at measured flows of ~ 500 m3/s. Measured velocities range from 0 (pink) to 3.8 m/s (red)

Lastly, the model monitor points were established. Placing a monitor point near the inflow and outflow allows the water-level elevations to be evaluated during the simulation. While the simulation runs, the water-level elevation at each monitor point is displayed and helps monitor simulation progress to evaluate the changes in the hydrograph inputs.

2.5 Sedimentological Modeling Parameters

SRH-2D offers a robust platform for modeling sediment transport scenarios. To conduct such studies, the workflow follows that of a hydraulic model with the exception of an important start condition and two additional parameters:

- Hydrologic Restart File,
- Define sediment boundary conditions, and
- Identify sediment materials input.

Perhaps the most important preliminary step for conducting a sediment transport analysis is the use of a restart file (RST file) before initiating a simulation. If no RST file is provided, meaningless erosion and/or deposition may occur in the time it takes for the hydraulic results to converge (Aquaveo, 2019). To prevent this miscalculation, a constant discharge of 500 m^3/s was simulated through the model domain until an equilibrium was obtained. The hydraulic results from this simulation were then used as the RST file for the sediment transport analysis.

The sediment boundary condition is a component to the hydraulic boundary condition that is activated once sediment transport simulations become of interest. Included within it are a suite of sediment transport formulas available for use within SRH-2D. The sediment boundary condition also permits two different ways for sediment inflow to be considered: "capacity" and "file". Selecting "file" requires an input file that contains a rating curve of sediment load (by fraction in m^3) versus the total water discharge (Aquaveo, 2019) Because no samples have been collected in this way, the "capacity" method was chosen that calculates the sediment transport capacity based on the element hydraulics, bed material gradation and the selected transport function (Aquaveo, 2019).

The sediment materials inputs were then identified. The Sediment domain is displayed in Figure 8. The area includes a portion of the main channel, the two channels feeding into the trenches, and the trenches. Areas were defined by erodible and non-erodible layers. The erodible surfaces constitute two layers of 1m and 20m thickness both with a density of 2650 kg/m^3. It's often recommended in SRH-2D that two layers be prescribed for sediment transport models, one to represent the active layer and the other to represent the subsurface layer (Aquaveo, 2019). The non-erodible area constitutes a single layer of 0.01m, using the same density and gradation curves, so that computation power can be directed to the area of interest. For both layers the gradation curves are the same (Figure 9). Because both the Parker equation and Wilcock-Crowe equation do not account for grain sizes less than 2mm, the gradation curve was modified to include only particles greater than 2mm. For consistency, the same grain size cut off was applied to MPM.

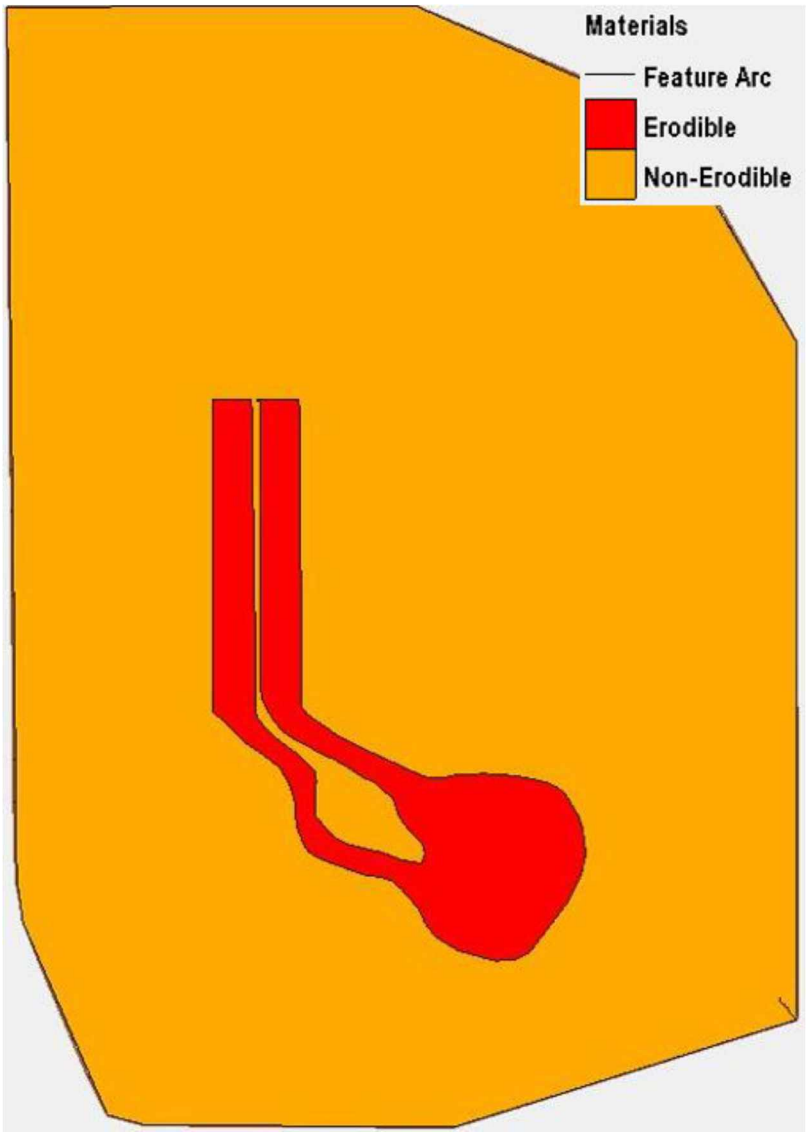

Figure 8: Sediment materials coverage denoting areas of active sediment transport

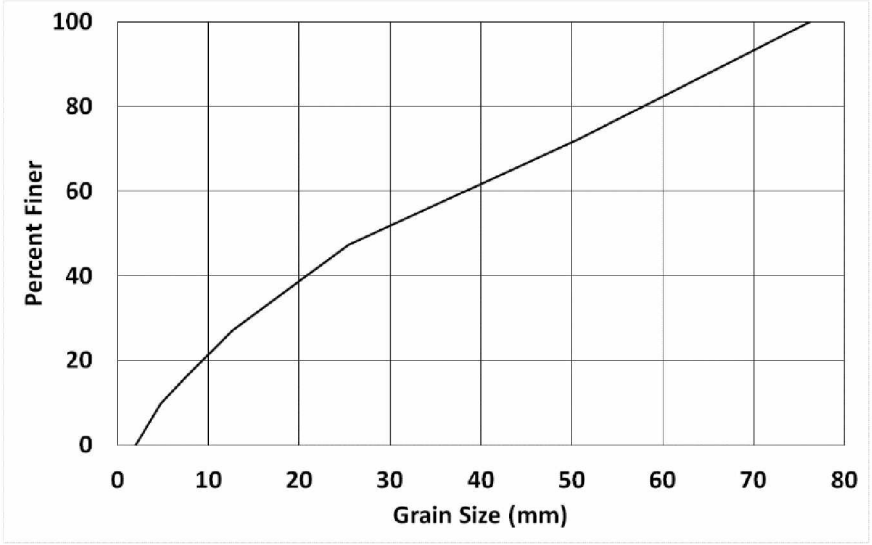

Figure 9: Model grain size distribution input

2.6 Hydrologic Scenarios Used

Each scenario considers a different hydrograph event that has previously occurred in the Sag River, where Figure 5 illustrates this comparison between scenario 1,2 and 3. Many, if not all uses of the SRH-2D model in the literature have been applied to more temperate river systems. As the Sag River resides in an Arctic environment, the surface is frozen for most of the year. To best approximate sediment transport with SRH-2D the river needs to be ice free. Therefore, the start dates of each scenario reflects the most likely period that the break up period has passed so there is not a significant quantity of ice left in the system. The end date for each scenario historically correlates with the minimum discharge of the year, suggesting sediment transport events past September 30th are minor.

The purpose of the selection of such hydrograph inputs for Scenario 2 and 3 is rooted in the implications for a warmer future. Discharge of Arctic river systems is strongly correlated to surface temperatures of their respective drainage basins. Peterson et al. (2002) found that an increase to global surface temperatures, over the past century, has caused Eurasian Arctic rivers to have an increase in discharge of roughly 2 km^3/year, from 1936 to 1999. Even further, using a stochastic sediment transport model, Sytski (2009) showed that there will be a 22% increase in the flux of Arctic river sediment for every 2°C increase in temperature and a 10% increase in sediment load for every 20% increase in discharge. Such trends found in the literature suggest that in the coming years, we would suspect larger amounts of discharge from Arctic rivers, the focus of scenario 2 and 3. By comparison,

scenario 1 was chosen based on the average cumulative volume of water to flow through the reach in a given summer from when data was first recorded for the Sag River. Matching it with the hydrograph that best represented this quantity, the year 1997 was chosen.

Chapter 3 - Results and Discussion

As mentioned before, three scenarios were simulated during the course of this work over the following time periods:

- Scenario 1: a "normal" cumulative volumetric flow
    - June 6th – September 30th, 1997
- Scenario 2: a maximum discharge event
    - June 6th – September 30th, 2002
- Scenario 3: the max cumulative volumetric flow
    - June 13th – September 30th, 2018

The findings are split into hydrologic results and sediment transport results, with a larger emphasis placed on the latter component. Hydrologic results consider velocity and water depth data during high and low flows for select time steps of the simulations. Sediment transport results include data derived from simulations of scenario 1. Results include a comparison made of the sediment transport equations showing the volume of sediment deposited in m^3, plan views of the model domain, profile views of each trench for each sediment transport equation, and the percentage of the trench filled after simulation completion.

To demonstrate the differences between each of the scenarios, three sediment transport equations were utilized: The Parker equation, the Wilcock-Crowe equation and the Meyer Peter and Müller equation.

3.1 Hydrologic Results

Outputs from a SRH-2D hydrologic model include water elevation, water depth, velocity, Froude, and shear stress. Figure 10 illustrates the variation in the velocity of scenario 1 for day 69 and day 71 of the simulations. During low flow, the largest velocity is approximately 1.6 m/s, generated in the main channel moving into the west channel inlet. Further, the water is near stagnation in the east trench, moving less than 0.1 m/s. During high flows, velocities exceeding 3 m/s are shown in the areas of the input channels to the trenches and in some areas of the trenches. Day 71 represents the largest flux of water of all the scenarios, inundating the full reach of the river. Figure 11 shows the same time periods for water depth. For low flows, the main river channel is only partially filled while both the west and east trench retain more water. However, the west trench input channel is between 1 m and 1.5 m deeper than the east trench, suggesting that when discharge is low, the bed elevation is such that there is a

disproportionate amount of water feeding into both trenches. This has repercussions for sediment transport simulations that will be discussed in the next section. By contrast, the high flows increase the water depth significantly across the domain, nearly converting the braided river into a single channel.

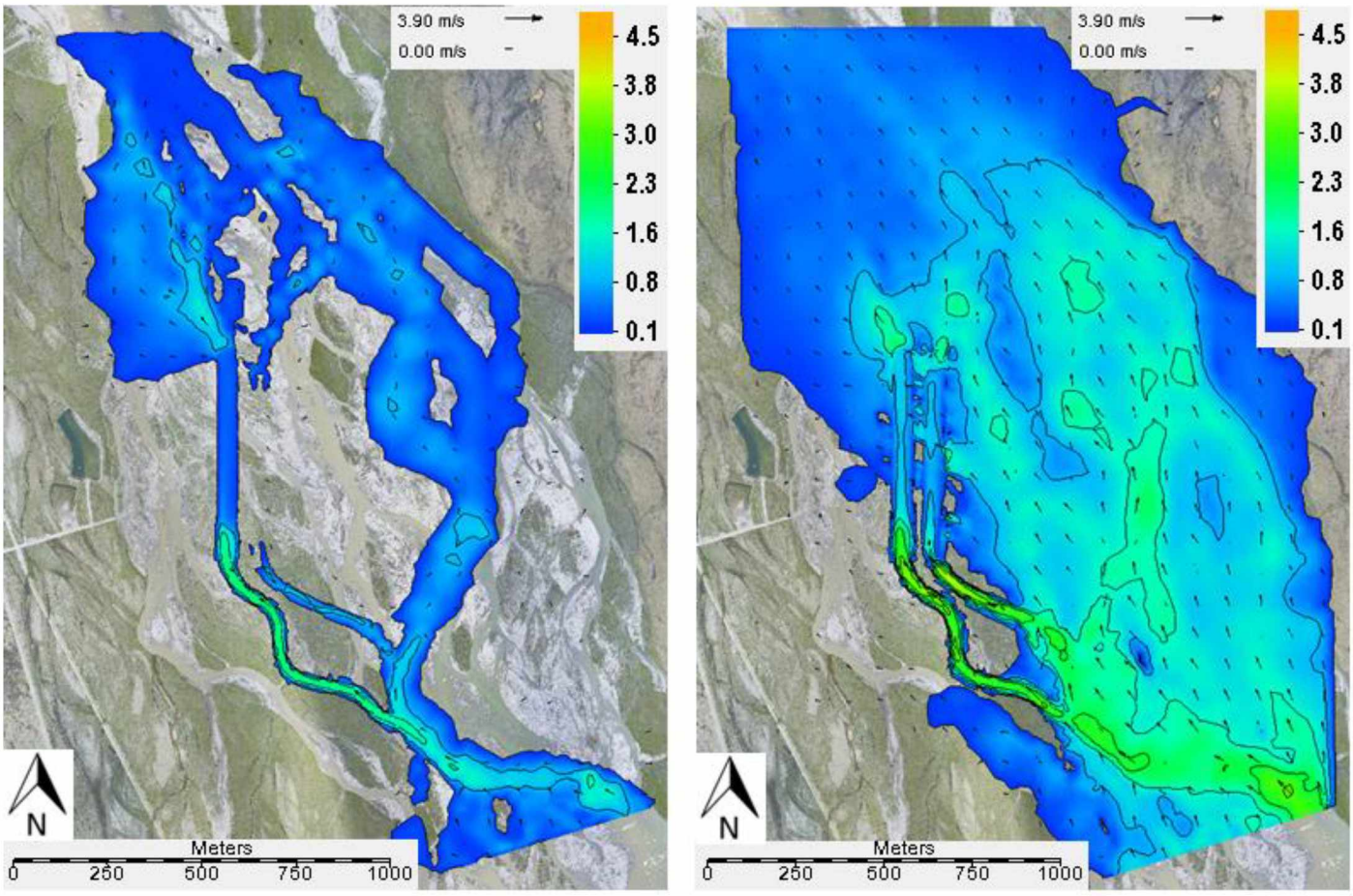

Figure 10: Scenario 2:(left) velocity magnitude (m/s) on day 69 (right) velocity magnitude (m/s) on day 71 during the peak event

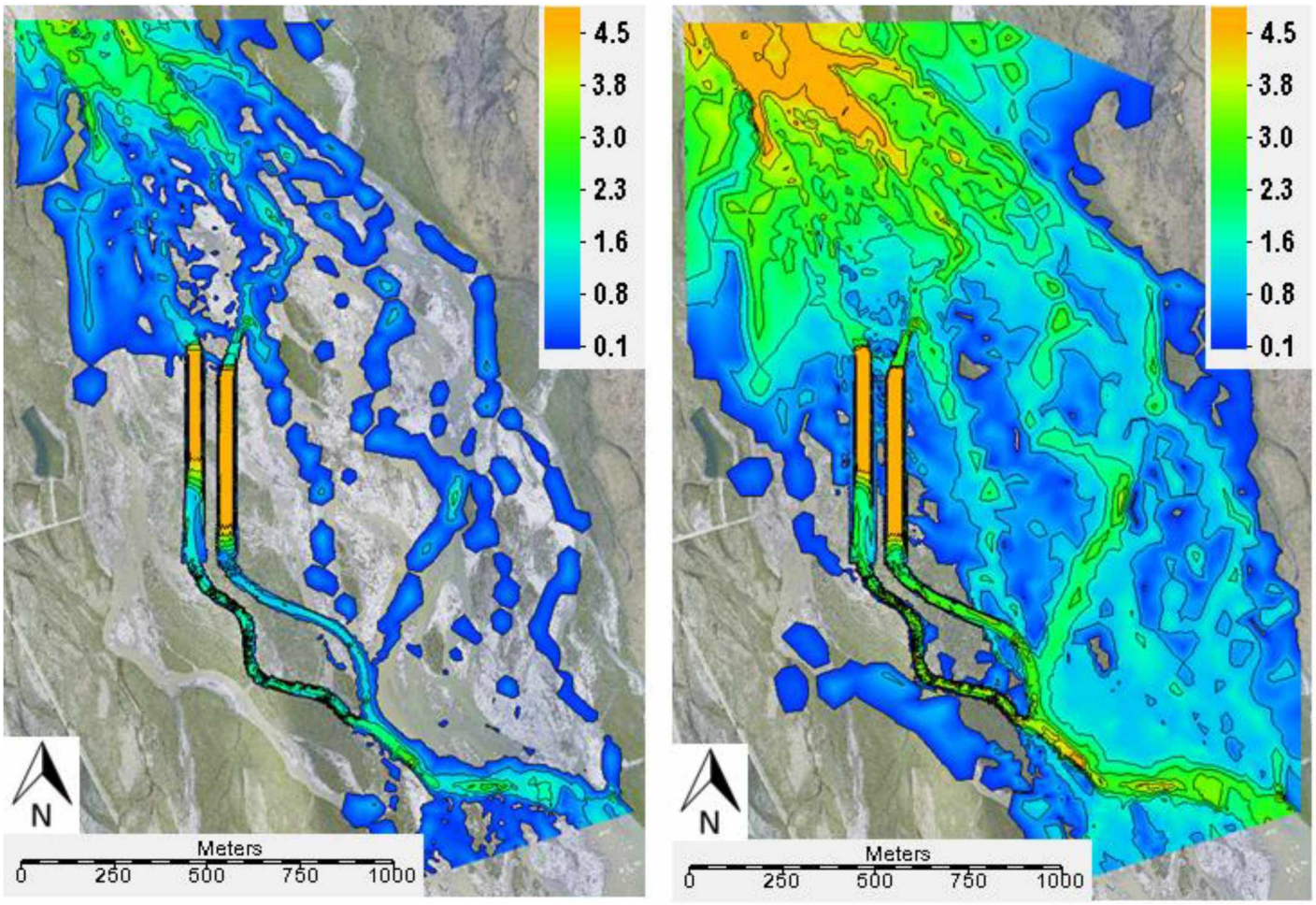

Figure 11: Scenario 2:(left) water depth (m) on day 69 (right) water depth (m) on day 71 during the peak event

3.2 Sediment Transport Results

Outputs from the sediment transport model include bed elevation, the evolution of d_{50} and the erosion depth. The main interest in the case of this study was a comparison between the bed elevations over the course of each simulation.

Findings from scenario 1 are presented as the baseline model from which scenario 2 and 3 can be compared with. To streamline the results and reduce redundancies in figures, the data observed from scenario 2 and 3 were placed in Appendix D and E respectively.

Figure 12 shows the variation in deposited trench sediment for the duration of the hydrograph. Periods where discharge approached or exceeded 750 m^3/s demonstrated the largest differences between each of the equations. At discharges less than 300m^3/s each sediment transport formula behaved similarly, predicting near equivalent sediment deposition. The difference was greatest for the

W-C equation that predicted lesser values of deposition most clearly seen in the east trench. Using the plan view from Figure 13, the difference in sedimentation confirms this. Both the Parker and MPM equations predicted larger quantities of sediment transport. In general, the higher discharges acted as a catalyst for sediment transport. This was especially true for the time around day 20 and day 60 during the simulation.

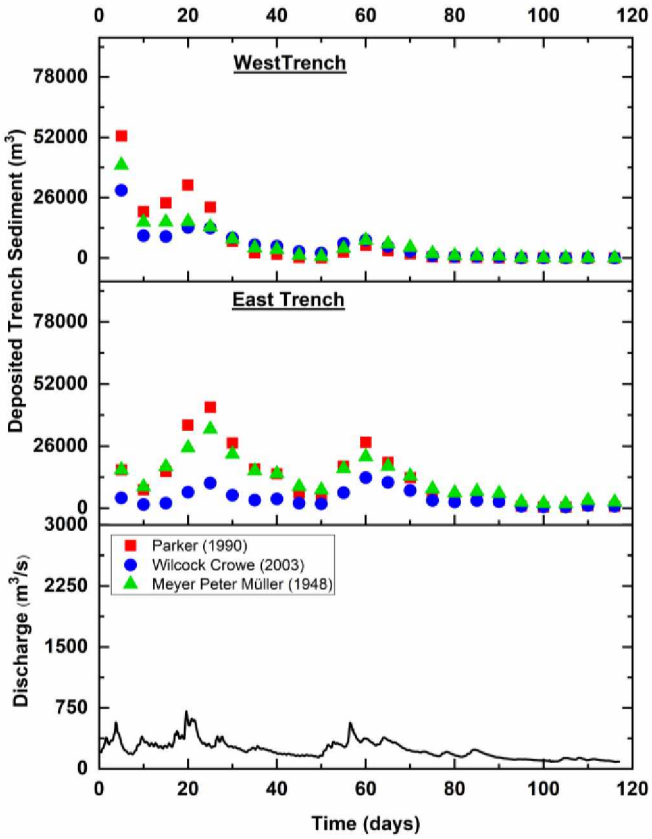

Figure 12: Deposited trench sediment in m^3 for east and west trench as compared to the scenario 1 hydrograph

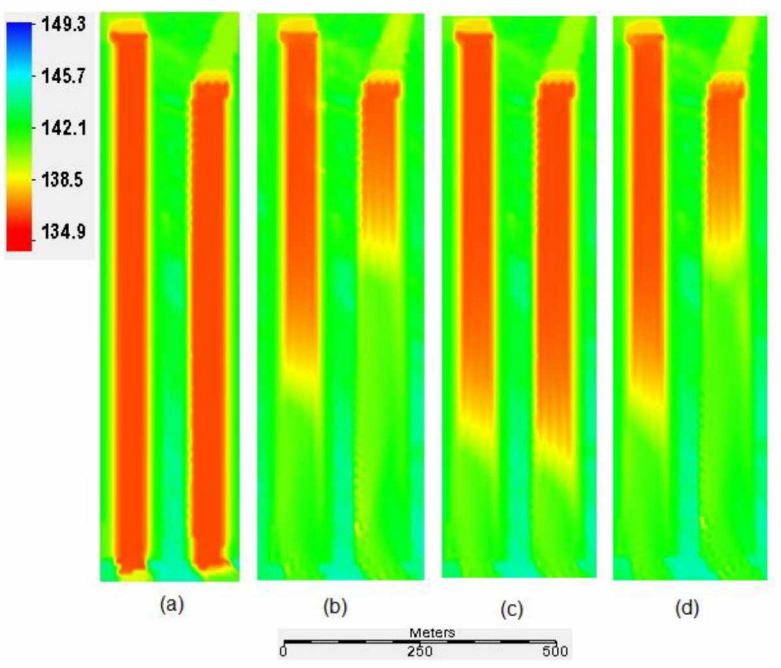

Figure 13: Comparison of bed elevation in meters. Far left, (a) is the initial elevation. The three figures right show the simulation end for (b) Parker Eq. (c) W-C Eq. and (d) MPM Eq.

Considering just the west trench, Figure 14 illustrates the rate of deposition for each equation as a time series profile view. Here the differences at each point during the simulation are more easily observed. Upstream of the trench, the erosion depth consistently increases, moving backwards in time. By day 116 the simulation end time is reached. Figure 15 shows the rate at which the trench is filled in percent. The Parker, W-C and MPM equations exhibit similar trends where the initial high flow leads to a large volume of sediment deposition. After day 20 though, the percent increase in trench sediment volume is much smaller. Comparing values to the east trench, the deposition pattern is quite different. By the end of the simulation for the east trench, both Parker and MPM predict it will be 70% filled while W-C predicts a much lesser percent fill of just over 20%. Ultimately, the fluxes of sediment erosion and deposition are strongly coupled with peaks in discharge.

Further, both the Parker and MPM equations predict the sediment deposition is nearly 30% greater for the east trench as compared to the west trench. One contributing factor leading to such large differences between the trenches could be the steeper slope for the upstream inlet to the trenches. The degree of slope is a primary factor of shear stress as well as water depth. Because the slope is much steeper for the east trench, the associated shear stress would also be much greater, prompting the

initiation of bed load movement. While the water depth is shallower in the east trench than in the west trench, the degree of slope, in this case, is more than enough to compensate for the lack of water depth. Though, both slope and water depth do not explain why the W-C equation predicts a much lesser quantity under the same conditions. This difference is likely associated with the difference in critical shear stress between the equations used. Wilcock et al. (2009) acknowledge that at different critical shear stresses, the transport behavior can change significantly based on the bed sand content.

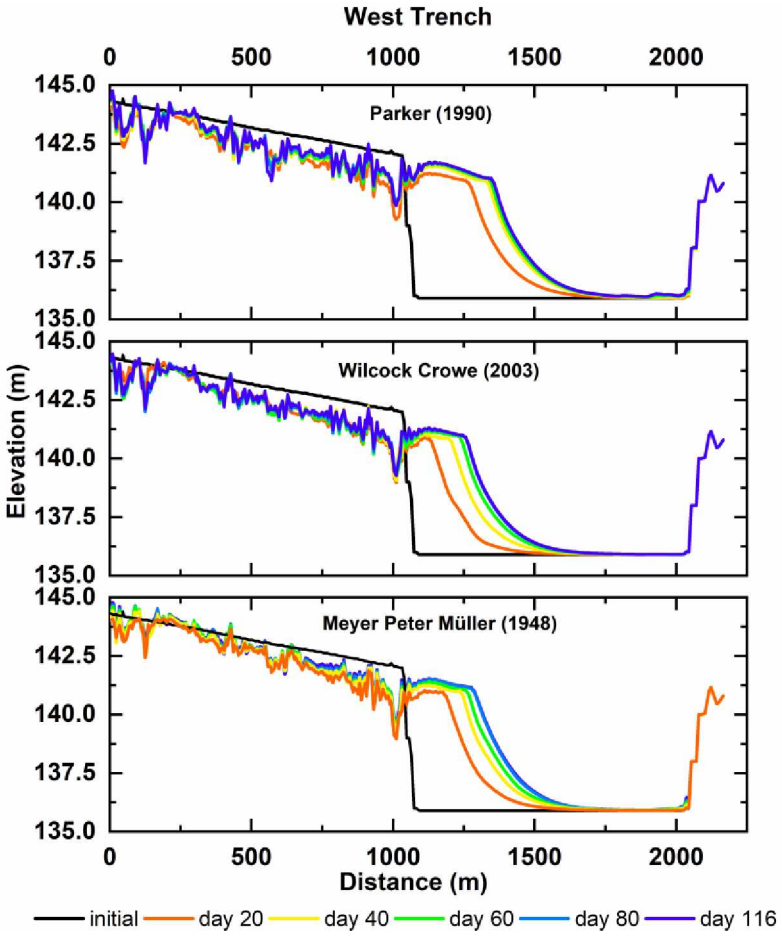

Figure 14: Time series of west trench comparing bed elevation for each sediment transport equation during scenario 1

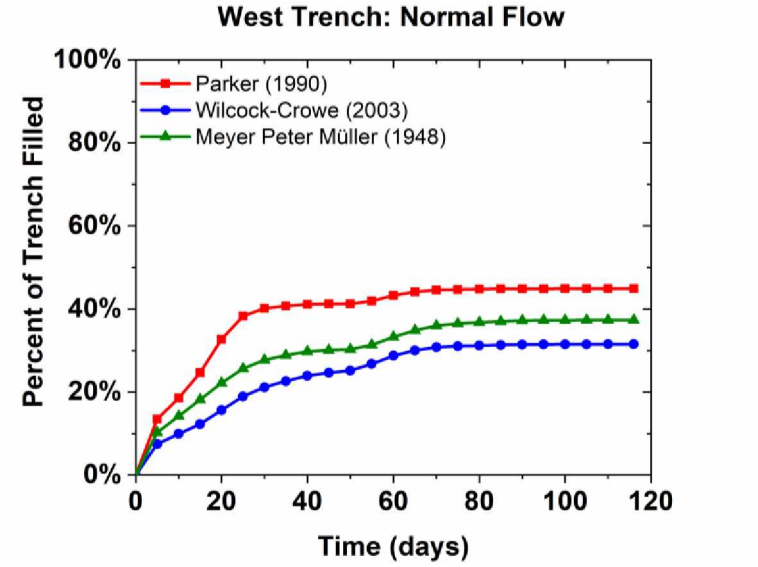

Figure 15: Percent of west trench filled during scenario 1

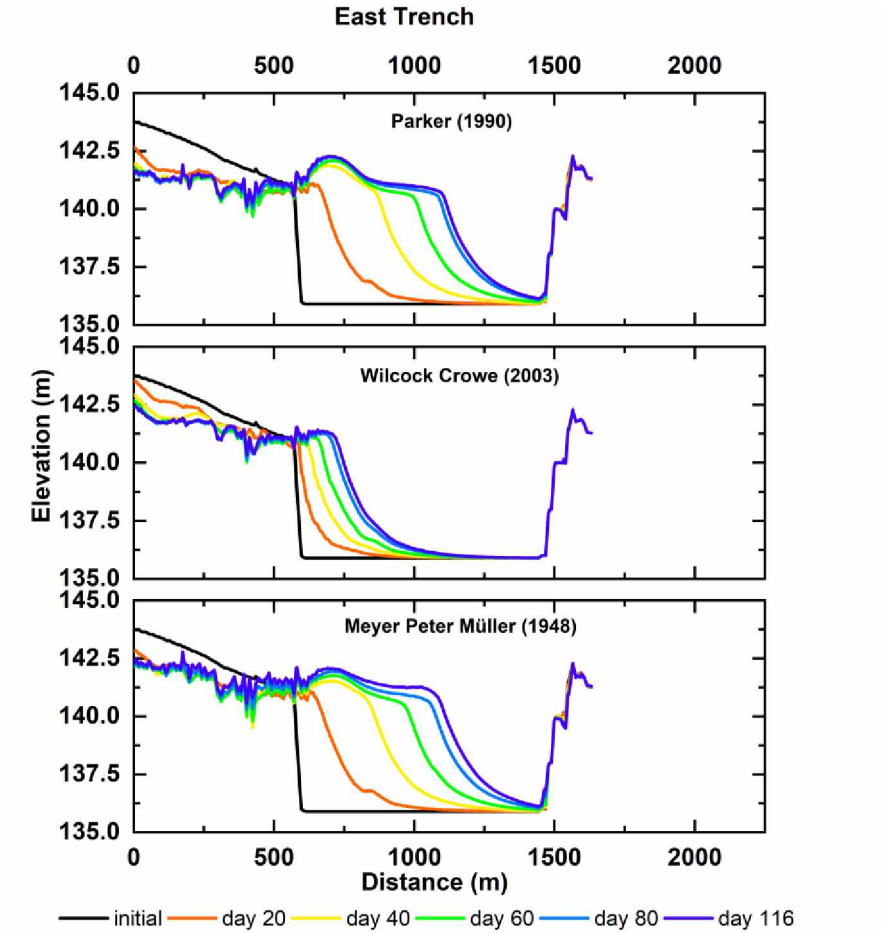

Figure 16: Time series of east trench comparing bed elevation for each sediment transport equation during scenario 1

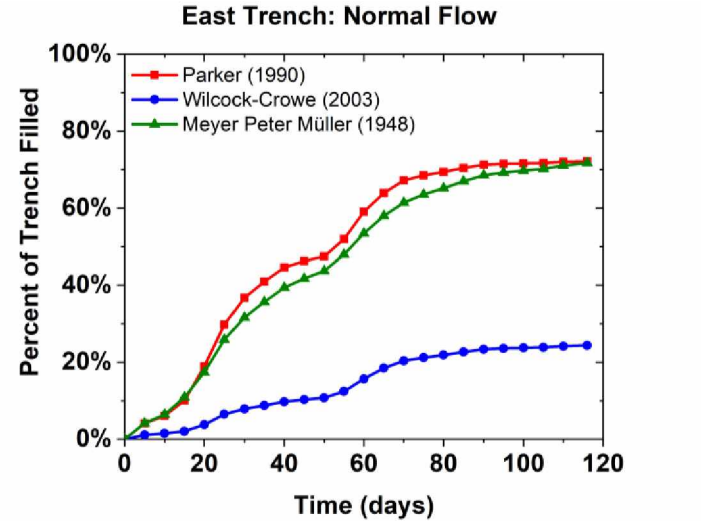

Figure 17: Percent of east trench filled during scenario 1

As a final comparison, Table 1 outlines the predicted sediment loads within the east and west trench at the end of the varying scenarios. Figure 18 outlines this same distribution of data except in percentage of each trench filled.

Table 1: Volume of sediment measured for each scenario under each equation

	West Trench Sediment (m^3)			East Trench Sediment (m^3)		
	Normal Volumetric Flow	Max Discharge Event	Max Cumulative Volume	Normal Volumetric Flow	Max Discharge Event	Max Cumulative Volume
Parker Eq.	175,560	250,524	286,986	282,040	63,133	403,621
W-C Eq.	123,249	161,576	135,275	95,303	43,964	135,275
MPM Eq.	146,020	238,524	406,085	280,191	157,009	439,609

What may not be as clear in Table 1 becomes clear in Figure 18, in that there are distinct differences in the percent filled for the east and west trenches. The only truly common trait for both the east and west trench is that if a substantial volume of water inundates the trenches, like scenario 3, the simulations suggest that they would be either filled or nearly filled in the span of a year.

The west trench follows a step like pattern for the Parker and MPM equations, progressing through the depiction shown in Figure 18, with the exception of the W-C equation, which predicted a lesser percentage filled for scenario 3. Based on the trend seen in the west trench, a linear relationship seems most fitting, advancing from scenario 1 through scenario 3.

However, this relationship is not as strong for the east trench. During scenario 2, an average of all three equations shows 33% less sediment deposition in the east trench. This difference is again directly correlated with slope and water depth, functions of shear stress. Observation of Figure 10 and Figure 11 show high velocities and deeper water depths for the west trench, suggesting a large discharge. Conversely, the same figures show slow velocities and shallow water depth for input into the east trench, suggesting a smaller discharge. While the slope is much steeper feeding into the east input channel, it is at an elevation that is slightly higher than the main channel, inhibiting flow to a degree and therefore reducing the water depth. Even more, once the discharge drops below 250 m^3/s, as it does a number of times during scenario 2, the flow into the east trench almost completely subsides. For both scenario 1 and 3, a discharge below 250 m^3/s happens much less frequently, which may suggest why the correlation between each scenario in the east trench is much less evident.

Using the results from scenario 1, the time for each trench to be filled was predicted with a linear approximation for the Parker, W-C and MPM equations (Figure 19 and Figure 20). Taking the average of each equation for the time in which the west trench takes to refill with upstream sediment yields approximately 2 years for both the east and west trench. Specific attention should be noted for the dashed green line. Because no corrections were provided to the original MPM equation within the numerical model outputs, the percent for which the trenches were refilled was halved as a proxy to the real correction outlined by Wong & Parker (2006) in an attempt to provide a better prediction to the time to fill each trench. This extended the average time to refill the west and east trench to about 2.5 years and 2.1 years respectively. The simulations for the normal cumulative volumetric flow suggests then that the trenches could refill on a timescale between 1.5-4 years for the west trench and about 1-3.75 years for the east trench with successive years of the same hydrograph input.

To compare the model results with physical results, during September of 2016, a pit was excavated further upstream of the model domain in an attempt to understand sequential years of sediment transport (Toniolo et al., 2018). In the time leading up to the summer of 2018, the pit had only been marginally filled. However, by October 25 of 2018, the pit had almost completely refilled, driven predominately by the 2018 max cumulative volume hydrograph, referred to as scenario 3 for this work (Figure 21). While the pit is much smaller in size than either of the trenches, it demonstrates that under significant discharge, copious amounts of bed sediment move, filling areas of lower elevation. This helps to validate the simulation outputs and show that a single year of high flows can lead to substantial sediment deposition.

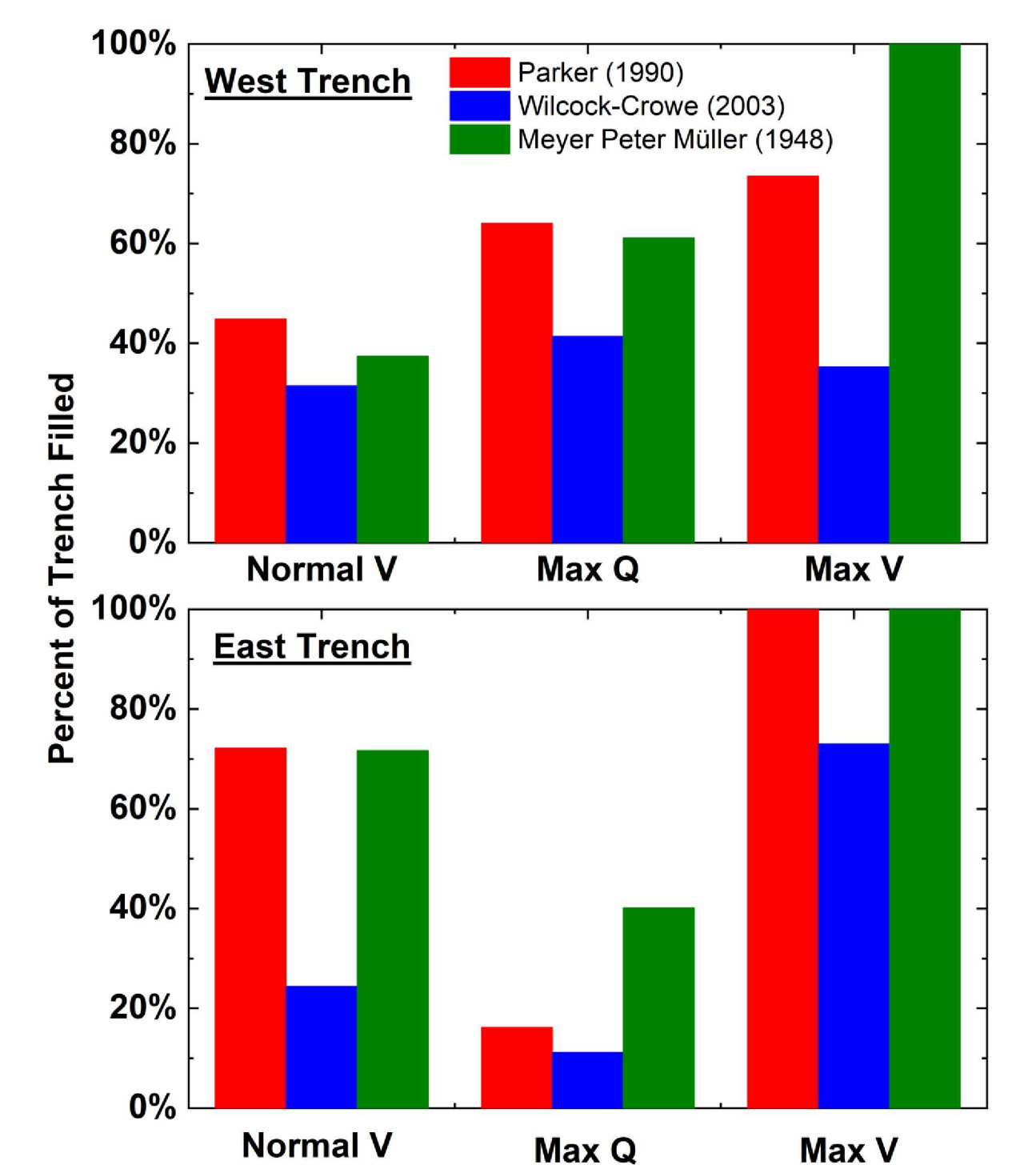

Figure 18: The percent of the west and east trench refilled for each scenario under each equation

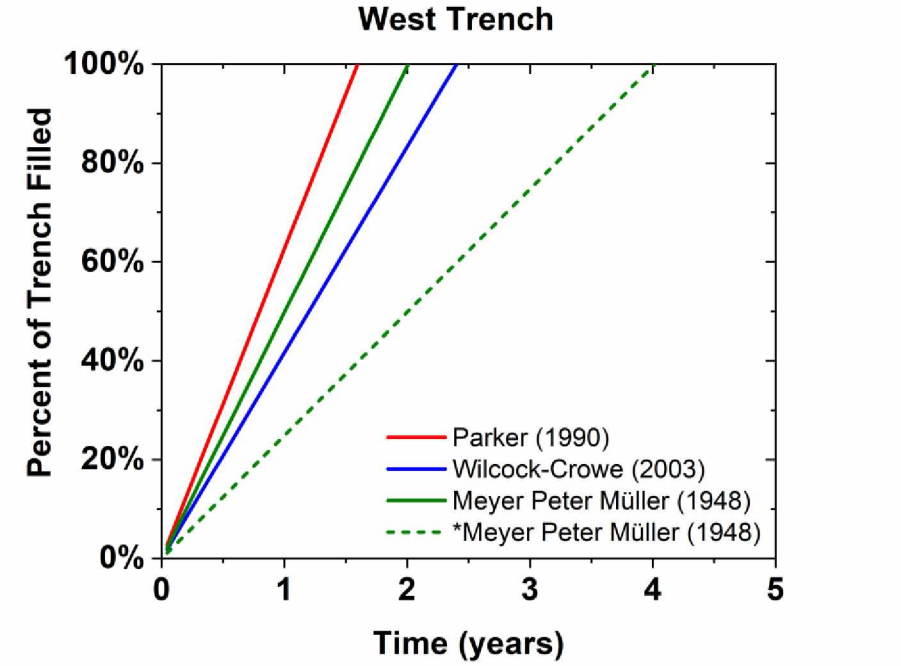

Figure 19: The time in years to fill the west trench based on a linear approximation of scenario 1 results (* denotes that the original Meyer Peter Müller results were halved in accordance with Wong & Parker (2006))

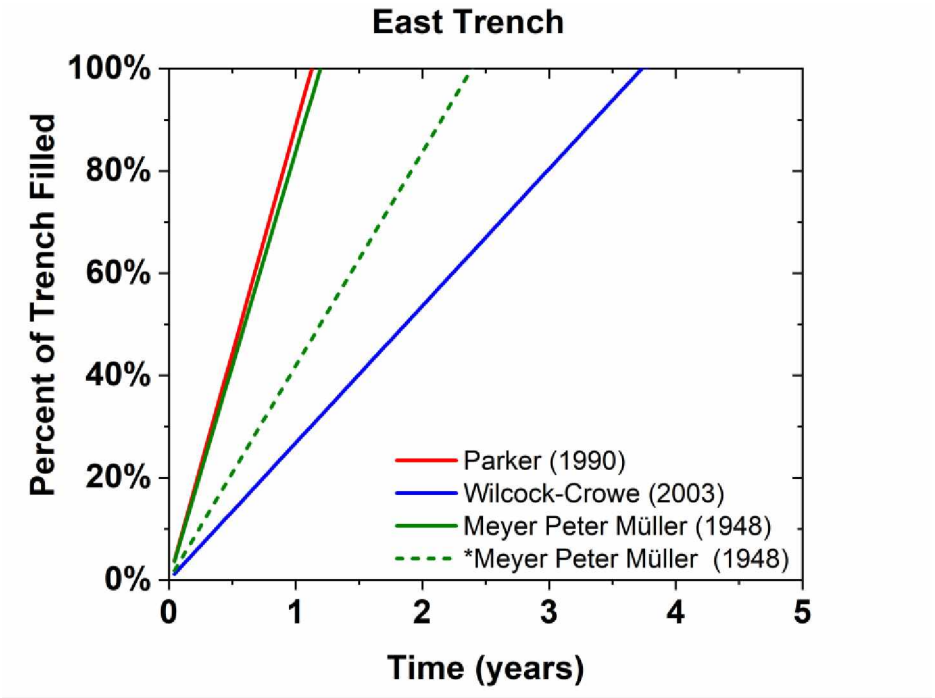

Figure 20:The time in years to fill the east trench based on a linear approximation of scenario 1 results(* denotes that the original Meyer Peter Müller results were halved in accordance with Wong & Parker (2006))

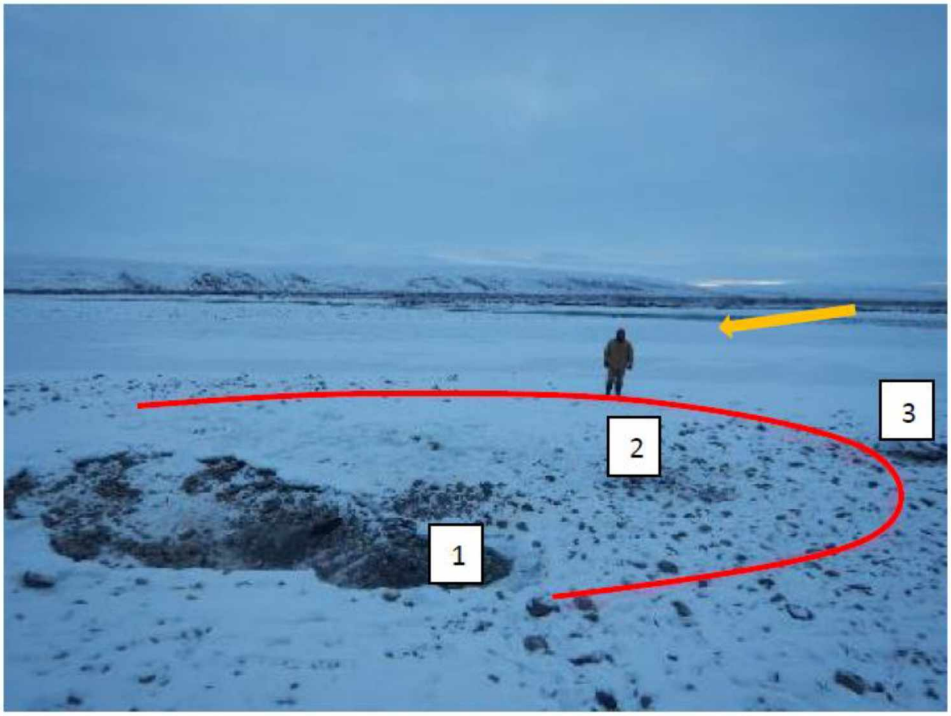

Figure 21: East view of pit on October 25, 2018 Pit remnant is visible at left. Red curve indicates approximate edge of pit as surveyed in September. Numbers indicate sediment sampling locations (Toniolo et al., 2018)

3.3 Modeling Assumptions and Limitations

As with all numerical modeling, the output results need to be observed cautiously. While most advanced 2-D models are robust, currently there is no simple method to completely capture the full complexity of sediment transport events. Additionally, under ideal conditions, field observations should be combined with computational modeling to achieve the most effective solution. However, given the remote location, the immense size of the river reach and arctic conditions of the site, field observations to support the modeling were limited. With that said, several assumptions were implemented where observations could not be obtained to fulfill the study objectives, along with some limitations, that are discussed below:

- A handful of other studies, concerning the selection of a Manning's roughness, mention that it can have a significant impact on sediment transport results for numerical modeling (Lai & Gaeuman, 2013;Moges, 2010; Lai et al., 2006). Many of these projects are done for single channel or slightly braided rivers, not for complicated braided river systems such as the Sag.

Constantly changing from one channel to another, the Sag can extend out to multiple kilometer wide reaches. While possible to conduct field work to identify roughness values, it is not viable to do a reach wide study to obtain them. Assumptions of their values, based on aerial imagery, therefore, is the best route to identify the boundary conditions for roughness values.

- For this model, the sediment materials boundary condition shown in Figure 8 was chosen to best illustrate erosion and deposition for the trenches out of interest of computing time. Therefore, erosion in the input channels could be an artifact of the limited sediment domain. While many factors contribute to the computing time needed to arrive at a solution, the effects seen in applying sediment transport to this model resulted in run times upwards of 3 days. The reality of sediment transport is that it occurs across the full extent of the river. However, it was not practical to run a complete sediment analysis across the entire model domain without unreasonably long run times.
- The original DEM where the trenches and input channels were designed to be placed had to be created using ArcGIS, meaning, the method by which the water inundated the trenches through inlet channels is a function of the user's decision. While the location of the trenches was known, there was no plan set created to route the water to the entrance of each trench. Therefore, the routes for the east and west trench were created to divert flow from the main channel in an attempt to achieve similar flow quantities. It has already been shown that there are considerable differences in deposition between both trenches due to differences in slope and water depth. Additionally, the channel dimensions feeding the trenches more closely resemble a rectangular channel than a braid in the river. Naturally, the width may vary moving downstream. With that said, depending on the methods of those creating them, the configuration of the input channels could be quite different both in the context of modeling and how they would physically be excavated.
- Additional limitations are imposed by the numerical model. While SRH-2D predicts the trench sedimentation fittingly, it fails to predict any significant amount of erosion on the downstream face of both trenches. Downstream of the eastern trench face in Figure 13 illustrates very little erosion, shown by the slight change in yellow hue from the initial condition to the simulation end for each equation. In reality, erosion under such conditions would be clearly observed. Reviewing literature, there is no clear mention of the use of a numerical model used to model

this type of situation, leaving the reason for a lack of erosion unresolved. Though, it is possible it could be a limitation of the fixed mesh. Lai (2017) showed in his work that certain limitations exist for both a fixed mesh and a moving mesh when modeling sediment transport. An additional limitation is that the model does not depict lateral migration, as it is a separate feature from the main SRH-2D model. Further research would be needed to investigate such effects.

- The Sag River is a highly braided river system spanning multiple kilometers at its widest reaches. As such, it is capable of changing its channel geometry in a short amount of time. With respect to the conditions of this model, the trenches fill with sediment under ideal conditions. At high peak events such as that of scenario 2, the large flux of associated sediment may cause more significant changes to the channel geometry in a way that could divert flow away from the channels that feed the trenches, disrupting the ideal conditions. Compounding this fact, additional changes to the channel geometry may propagate from the trench excavation process. Therefore, in the case of this project, monitoring of the site will provide the best details to future changes and accuracy of the model results.
- Perhaps the largest limiting factor is that there is no way to predict the tendency of future annual discharges. Scenario 1, 2 and 3 were meant to capture a range of historical events that have occurred since record keeping began on the Sag. However, without knowing future flow conditions, the time for which the trenches will be refilled is equally unknown. Ultimately, records of past hydrographs cannot accurately predict what may happen in the future. Persistent monitoring of the site will largely be necessary to understand how the trenches will refill.

While many assumptions and limitations are present throughout this work, this was the first time that a temporal solution has been achieved through modeling, regarding gravel mining operations done in the Sag River. The work done here provides the grounds for a quality comparison of each of the investigated scenarios. Consequently, it should provide a springboard for future modeling. However, as mentioned by Lai et al. (2006), caution is urged in observing the absolute sediment transport rate and deposition amount recorded, because without physically measured values for comparison, it can contain a high degree of uncertainty.

Chapter 4 - Conclusions and Future Work

4.1 Conclusions

The SRH-2D numerical model was used in conjunction with the SMS graphical user interface to evaluate sediment transport under three varying scenarios starting in June and ending in September for 1997, 2003 and 2018. As a robust 2-D model, it suitably captured the complexity of the Sag River.

The goal of these simulations was to address the time it would take for two trenches in the Sag River, near MP 366 of the Dalton Highway, to refill with upstream sediment. Three varying scenarios were observed where for each scenario the Parker, W-C and MPM sediment transport equations were applied. Figure 18 illustrates the percentage that the east and west trenches are filled for each scenario for each respective sediment transport equation. Both the slope and water depth vary for the channels feeding into the east and west trench. Because shear stress is a function of both slope and water depth, factoring into sediment transport, the results demonstrate considerably different rates of deposition in each trench for the same input hydrograph. Ultimately, it was found that if sequential years similar to scenario 1, occur the east and west trenches fill between 1.5-4 years and 1-3.75 years respectively. Under scenario 2 the time to fill would be an even shorter period (Figure D.4 and Figure D.6) while scenario 3 would reflect the shortest time to fill, where most simulations of the different equations suggest both trenches would fill to nearly 100% in the span of one year (Figure E.4 and Figure E.6)

Though the time to fill each trench is based on simulations, evidence from past gravel extraction along the Sag River has shown that the presented time window is entirely plausible. In 2008, a similar gravel extraction was conducted further upstream of the study site along MP 334 of the Dalton Highway. Six years later, the main channel migrated from east to west and began flowing through the former main extraction pit (Toniolo et al., 2017b). In that time, a gravel bar had formed in the exact location of where the extraction had been done, suggesting the site had been filled.

In this work, many assumptions and limitations were discussed. Still, the important information to garner from this study is that this is first time an estimate has been provided for gravel mining activity in the Sag River.

4.2 Future Work

What may prove most useful from the extent of this work is the development of a management tool for future material sites along the Sag River. The necessity for gravel extraction dates back to the time the Alaska pipeline first began construction and it's likely then that gravel mining will continue into the

future. Because this model is the first of its kind on the Sag River, it could be transformed into a tool to predict when future extraction sites have refilled. In this way, the permitting process can be expedited rapidly, saving time and relieving the need for obtaining additional permits for new extraction sites by returning to sites where the paperwork has already been conducted.

Additionally, knowing the estimated time to fill may also provide ecologists with information to know how the wintering grounds for fish habitats may change as the trenches begin to refill. In this way, studies could be done to better understand the local fish populations and the role the trenches may play during the winter months.

Currently, a sediment transport equation is in development to fit the morphological conditions of the Sag River based on collected field work. Once the equation is fully developed, it could be coupled with more exact field measurements to provide a more refined analysis for the time an extraction site takes to refill.

Chapter 5 - References

Aquaveo. (2019). SMS:SRH-2D. Retrieved from https://xmswiki.com/wiki/SMS:SRH-2D

Chow, V. T. (1959). *Open-Channel Hydraulics*. New York: McGraw-Hill.

Galay, V. J. (1983). Causes of River Bed Degradation. *Water Resources Research*, *19*(5), 1057–1090.

Lai, Y. G. (1997). An unstructured grid method for a pressure-based flow and heat transfer solver. In *Numerical Heat Transfer, Part B* (pp. 267–281).

Lai, Y. G. (2000). Unstructured grid arbitrarily shaped element method for fluid flow simulation. *AIAA*, *38*(12), 2246–2252.

Lai, Y. G. (2008). *SRH-2D version 2: Theory and User's Manual*. Denver: Technical Service Center, Bureau of Reclamation, Denver, CO.

Lai, Y. G. (2010). Two-Dimensional Depth-Averaged Flow Modeling with an Unstructured Hybrid Mesh. *Journal of Hydraulic Engineering*, *136*(1), 12–23. https://doi.org/10.1061/(ASCE)HY.1943-7900.0000134

Lai, Y. G. (2017). Modeling Stream Bank Erosion : Practical Stream Results and Future Needs. *Water*. https://doi.org/10.3390/w9120950

Lai, Y. G., Weber, L. J., & Patel, V. (2003). Nonhydrostatic three-dimensional method for hydraulic flow simulation. II: validation and application. *Journal of Hydraulic Engineering*, *129*(3), 206. https://doi.org/10.1061/(ASCE)0733-9429(2003)129:3(206)

Lai, Y. G., Holburn, E. R., & Bauer, T. R. (2006). *Analysis of Sediment Transport Following Removal of the Sandy River Delta Dam*.

Lai, Y. G., & Gaeuman, D. (2013). *Bedload Adaptation Length for Modeling Bed Evolution in Gravel-Bed Rivers (Interim Report)*.

McLean, R. (1993). *North Slope Gravel Pit Performance Guidelines*. Fairbanks, Alaska.

Meyer-Peter, E., & Müller, R. (1948). Formulas for bed-load transport. *IAHR*, 39–64.

Moges, E. (2010). *Evaluation of Sediment Transport Equations and Parameter Sensitivity Analysis Using the SRH-2D Model*. University of Stuttgart. https://doi.org/10.1021/jacs.5b00200

Parker, G. (1990). Surface-based bedload transport relation for gravel rivers. *Journal of Hydraulic Research*, *28*(4), 417–436. https://doi.org/10.1080/00221689009499058

Parker, G. (2008). Transport of Gravel and Sediment Mixtures. In M. García (Ed.), *Sedimentation Engineering* (pp. 165–253). Reston, Virginia: American Society of Civil Engineers.

Peterson, B., Holmes, R., McClelland, J., Vorosmarty, C., Lammers, Richard, Shiklomanov, A., Shiklomanov, I., & Rahmstorf, S. (2002). Increasing river discharge to the Arctic Ocean. *Science*, *298*(December), 2171–2173.

Rodi, W. (1993). *Turbulence models and their application in hydraulics* (3rd Editio). Balkema, Rotterdam, The Netherlands: IAHR Monographs.

Sytski, J. P. (2009). Sediment discharge variability in Arctic rivers: implications for a warmer future. *Polar Research*, (September), 8369. https://doi.org/10.3402/polar.v21i2.6494

Toniolo, H., Stutzke, J., Lai, A., Youcha, E., Tschetter, T., Vas, D., … Irving, K. Antecedent Conditions and Damage Caused by 2015 Spring Flooding on the Sagavanirktok River , Alaska (2017a). https://doi.org/10.1061/(ASCE)CR.1943-5495.0000127.

Toniolo, H., Youcha, E. K., Tape, K. D., Paturi, R., Homan, J., Bondurant, A., … LaMesjerant, E. (2017b). *Hydrological, Sedimentological, and Meteorological Observations and Analysis on the Sagavanirktok River 2017 Interim Report*.

Toniolo, H., Youcha, E. K., Tape, K. D., Bondurant, A., Lamesjerant, E., Ladines, I., … Laurio, J. (2018). *Observations and Analysis of the Sagavanirktok River 2018 Interim Report and Analysis of the Sagavanirktok River 2018 Interim Report*.

Wilcock, P. R., & Crowe, J. C. (2003). Surface-based transport model for mixed-size sediment. *Journal of Hydraulic Engineering-ASCE*, *129*(2), 120–128. https://doi.org/10.1061/(ASCE)0733-9429(2003)129

Wilcock, P. R., Pitlick, J., & Cui, Y. (2009). *Sediment Transport Primer: Estimating Bed-Material Transport in Gravel-bed Rivers*. Fort Collins, Colorado.

Wong, M., & Parker, G. (2006). Reanalysis and Correction of Bed-Load Relation of Meyer-Peter and Müller Using Their Own Database. *Journal of Hydraulic Engineering-ASCE*, *132*(November), 1159–1168.

Appendix A Trench Creation

In order to first construct each trench they were drawn up in AutoCAD. Utilizing the plan and profile views of the mining and reclamation plan provided by Cruz the trenches were drawn following the dimensions provided. Included below are the plans. The lines used to construct each cell were duplicated across the span of each and then divided to create a consistent spread of points (Figure A.1). To assign the trenches the proper geographic coordinates a feature in AutoCAD allowed the input of coordinates to geo reference one location of the drawing. Considering the southeast corner of the east trench, the latitude and longitude were extracted from Google Earth in close proximity and provided for this point. An oblique view of the trenches is given below. The drawing could then be saved in preparation for the next step.

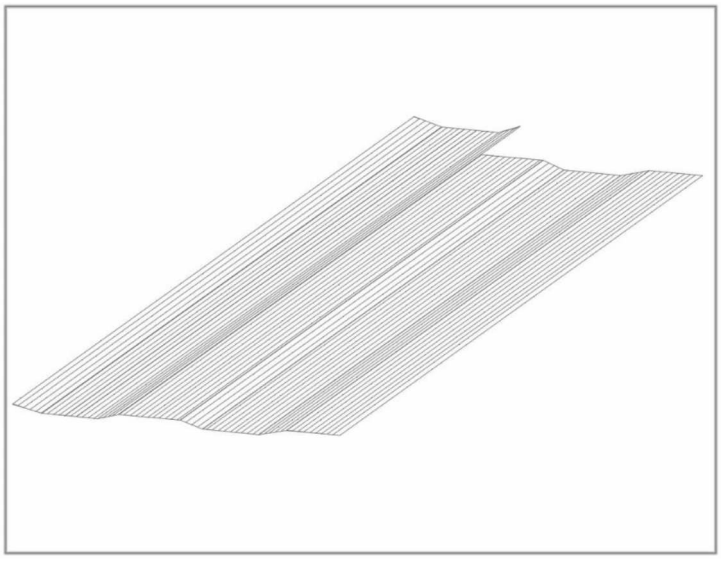

Figure A.1: Oblique view of trenches drawn in AutoCAD

To ensure the drawing file from AutoCAD was correctly positioned the TIF (image file) of the portion of the sag was imported into ArcGIS for reference. By utilizing the raster accompanied with the TIF the elevation of the original chosen point of the SE corner of the east trench could be obtained. Because the trenches were previously drawn in a free space the measured elevation of each point was from a datum of zero. By defining the reference point from the corresponding raster location the specific elevation could be rewritten to match the study site. In this way, the remaining points could be rewritten to have the correct elevation based off this singular point by simply adding or subtracting

from the reference point in the point spread. This same procedure was executed for marking the latitude and longitude of each point. From here, the points could be converted into a single cohesive polygon

Following the creation of the trenches, four channels were created to provide the water a corridor to travel in and out of the cells. The southwest input channel followed a braid of the river already present but because the eastern trench lacked the presence of an input channel, one was constructed in an attempt to provide the flow with the least amount of resistance to the trench input. To ensure that it obtained a near equal flow compared to the southwest input, the southeast input also utilizes discharge from the main channel of the Sagavanirktok. The depth of each segment for the channel inputs and outputs were prescribed a singular elevation for each polygon where each step between polygons is a gradual drop in elevation feeding into the trenches and then a slight rise leaving the trenches.

Once each point was issued an elevation and a location a series of raster math calculations were used to subtract out the area within the previously constructed DEM that the trenches and input channels would replace. Having completed the modifications to the terrain, the newly created DEM could be saved and imported into the modeling software. Figure A.2 shows the scatter data comparison of same area with and without the trench and input channels in the model domain.

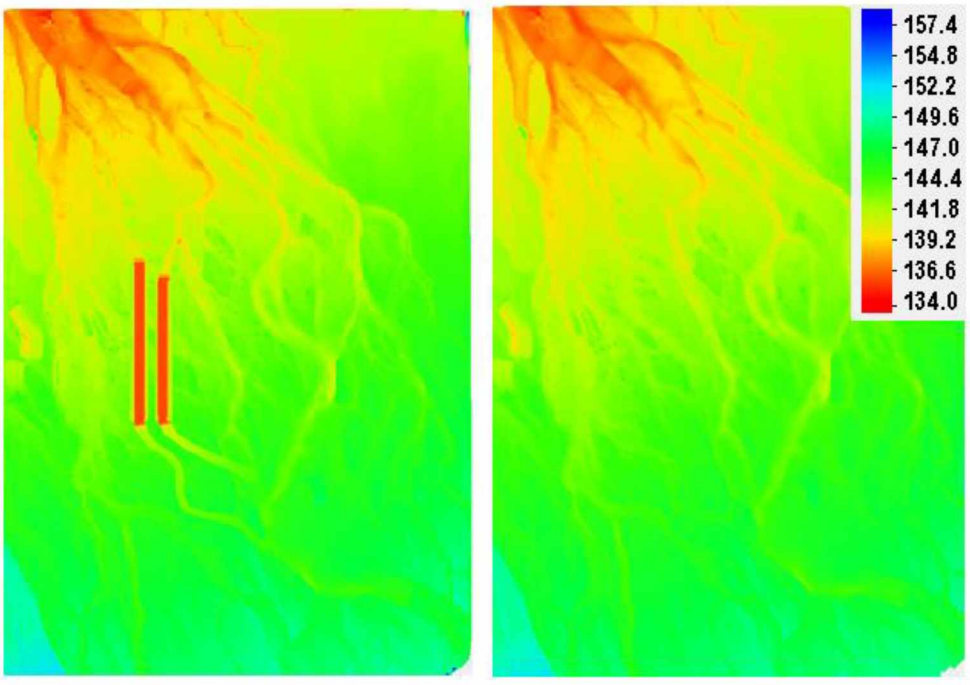

Figure A.2: Comparison of model domain with trenches and without trenches measured in meters

Appendix B Model Mesh Evolution and Configuration

Three preliminary meshes of varying sizes were tested to balance time efficiency and accuracy. Each evolution of the mesh shares similar features. Shown in Figure B.1, the triangular element count progresses from (a) 24121 to (b) 17837 to (c) 16335 to (d) 19269. As an anecdotal and experience based guideline for sediment transport simulations, its often recommended that fewer than 20,000 elements are used to limit computation time (Aquaveo, 2019). Based on the three initial meshes, Figure B.1(d) improved overall accuracy of flow into the trenches while adhering to the recommended element count. As a check, three hydrologic flow simulations of the three previous meshes were compared for two arcs drawn through two channels of the river reach Figure B.2. Since the major focus of these simulations is aimed at visualizing the deposition and erosion of sediment in the trenches, the mesh with the largest element size spacing west of the trenches, in the main channel, was chosen because of the similarity in water depth between the hydrologic simulations (Figure B.3 and *Figure B.4*). In other words, because there was no significant loss in definition by reducing the number of elements, Figure B.1(d) was chosen to represent the final model domain mesh, as it highlighted the area of interest.

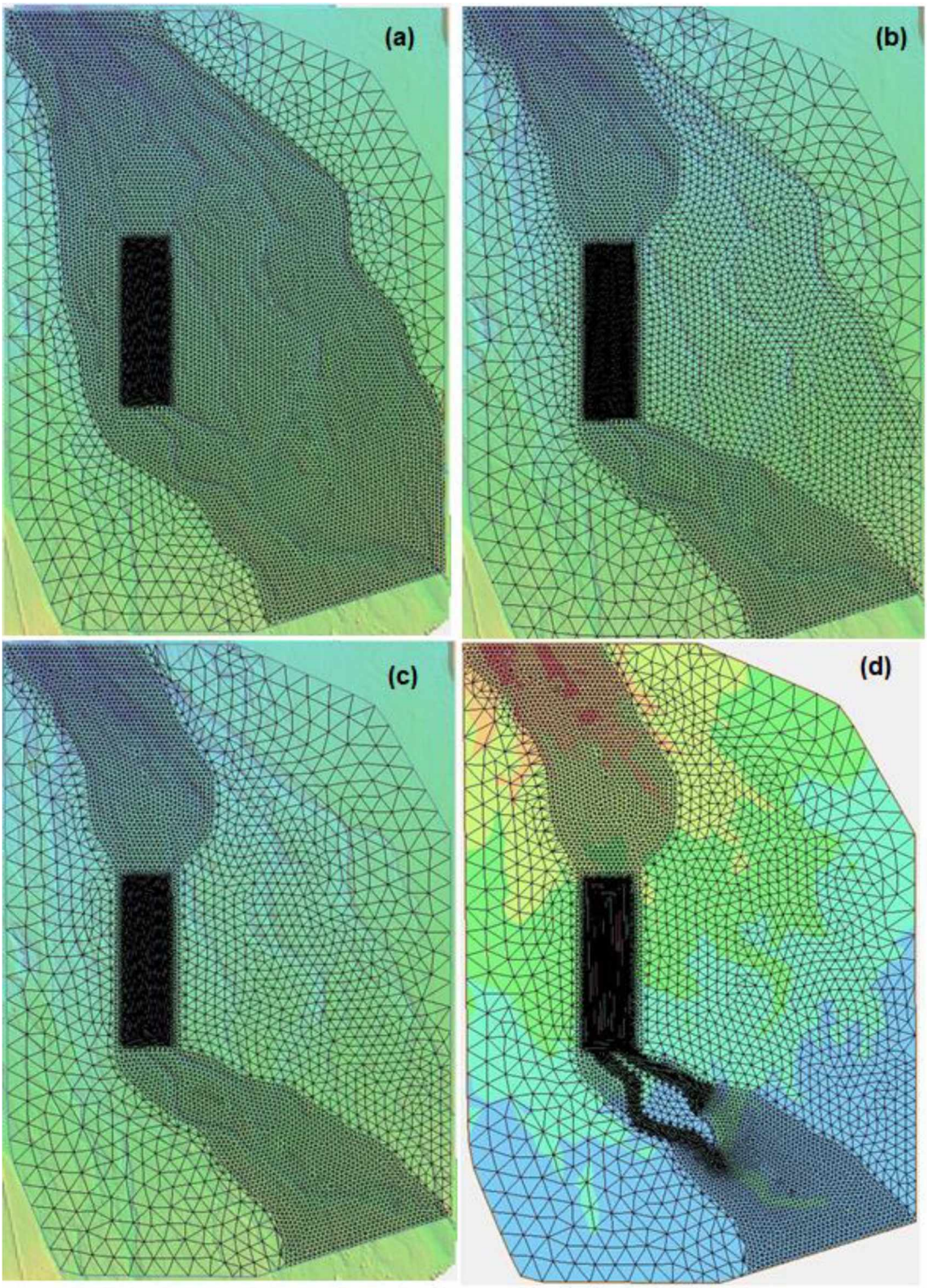

Figure B.1: (a) preliminary mesh (b) 2nd mesh (c) 3rd mesh (d) final mesh

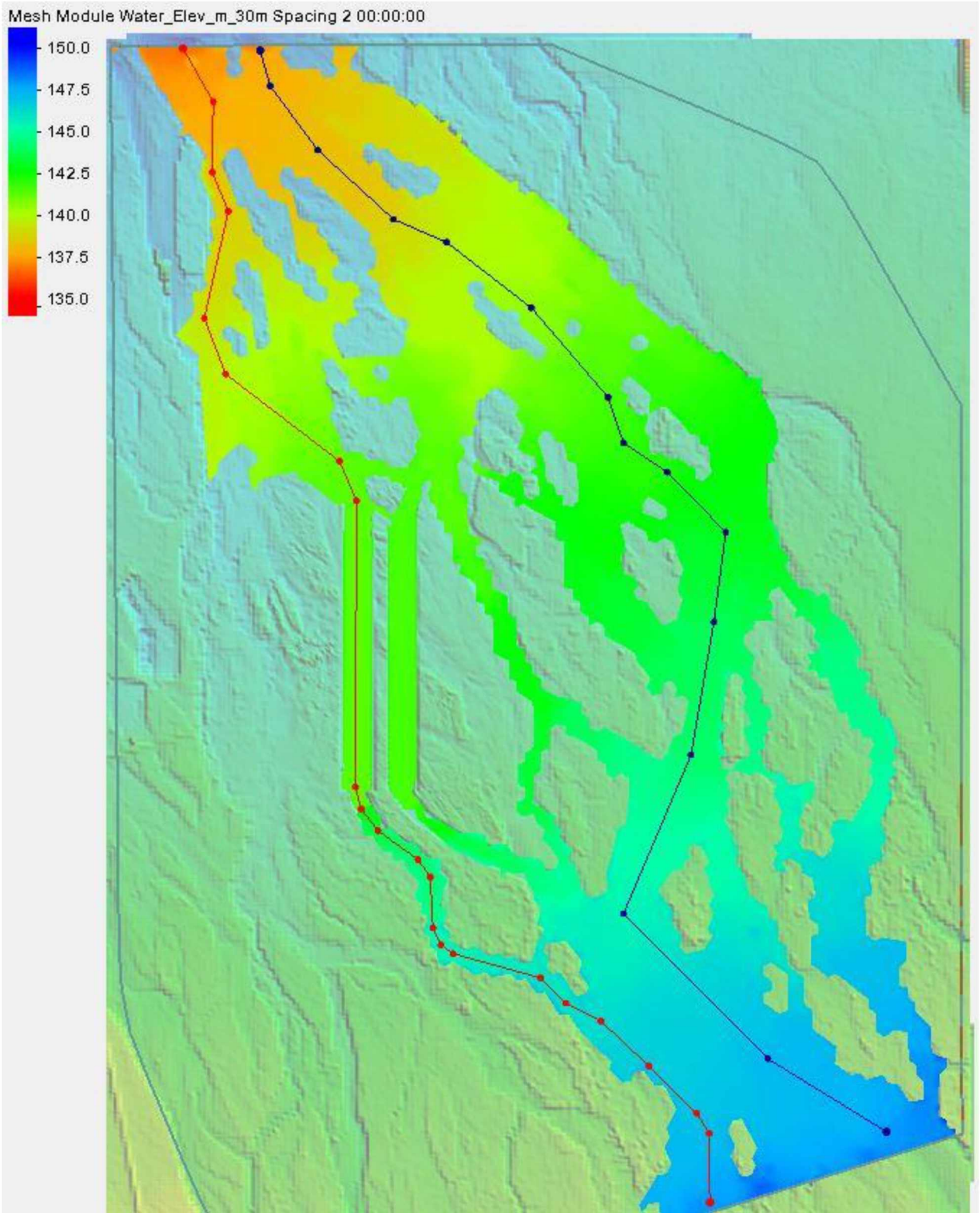

Figure B.2: Plan view of model domain showing arcs through the west trench and through the main channel

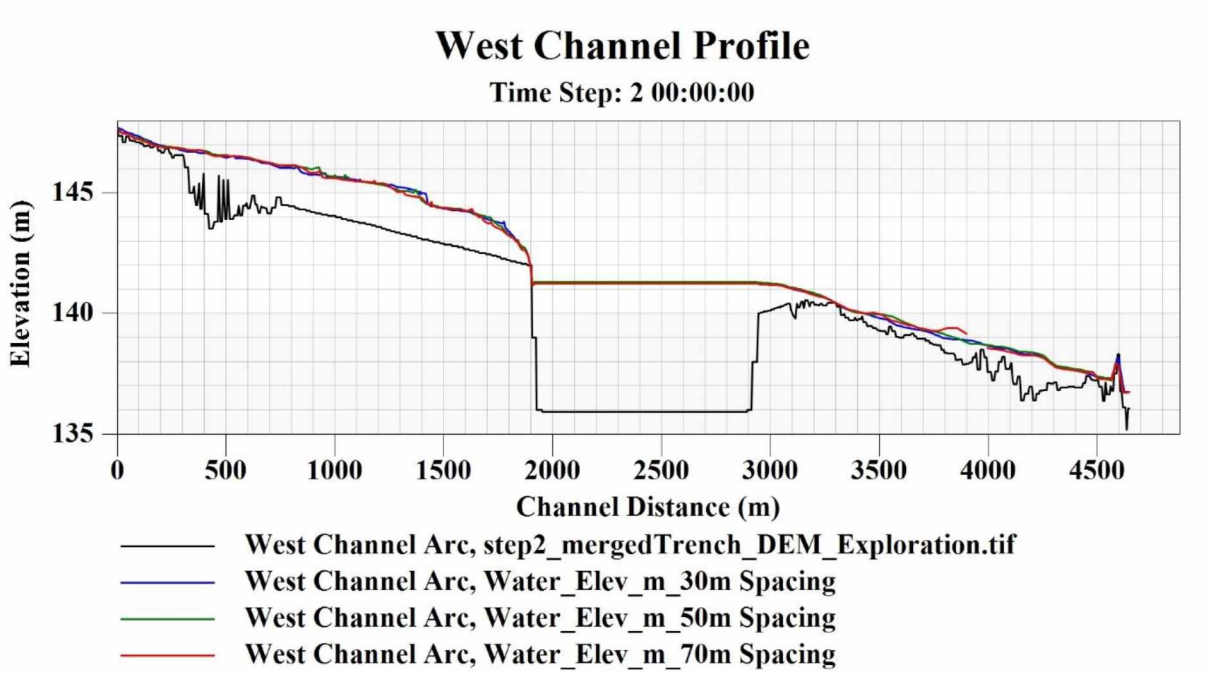

Figure B.3: West channel profile from Figure B.2 comparing the three preliminary meshes

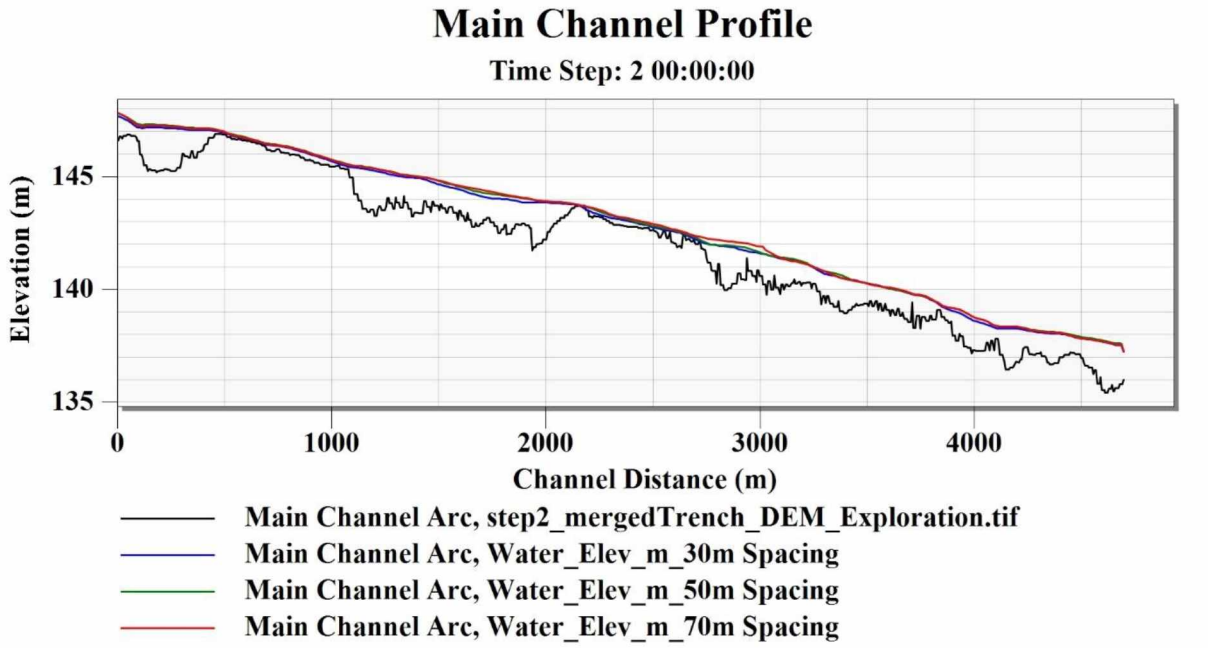

Figure B.4: Main channel profile from Figure B.2 comparing the three preliminary meshes

Appendix C Sediment Transport Equation Parameters

For each sediment transport equation, there are unique values neccesary as inputs to run the model.

In utilizing the Parker equation there are two transport equation coefficients that are generally unique to the chosen river defined as: θ_c (represented as τ_c^* in other literature) , the critical shear stress value above which sediment is mobilized and α, the exposure factor compensating for critical shear stress reduction of large particles and increase in critical shear stress for smaller particles. The chosen values are shown in Figure C.1.

Three transport equation coefficients are required for the W-C equation: Wilcock T1 coefficient, Wilcock T2 coefficient and the Wilcock sand diameter. Model input values for these parameters are shown in Figure C.2. The Wilcock Sand diameter was set to 2 with the understanding that the smallest particle size for this study was 2 mm. The other coefficients were left as the default values provided in the program.

Only one transport equation coefficient is applied to the MPM equation shown as the Meyer Peter Müller hiding factor. Figure C.3 shows chosen value.

Besides the unique coefficients to each equation, there are a few non-transport equation dependents that are standard across each equation: water temperature, adaptation length for bed load transport and active layer thickness specification. Details regarding these values are in the latter half of Figure C.1, Figure C.2 and Figure C.3. Water temperature, for this model, is used to compute water viscosity that is used to establish sediment fall velocity. The adaptation length for bed load transport was set at a constant length. Lai & Gaeuman (2013) demonstrated the sensitivity of this parameter and that the results should be investigated cautiously. The active layer thickness was represented by thickness based on d_{90}. Adhering to the recommendation of keeping the thickness from 1 to 3 times the d_{90} for gravels, the thickness was set to 100mm, approximately 1.5 times the d_{90} of the model grain size distribution (Aquaveo, 2019).

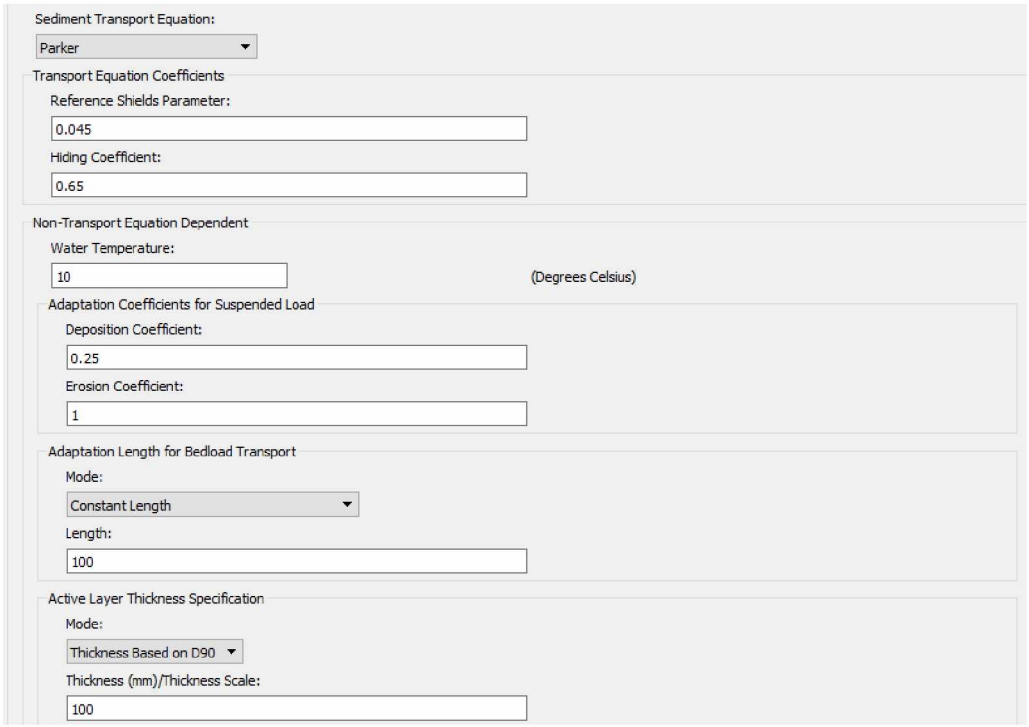

Figure C.1: Transport equation coefficients for the Parker equation and non-transport equation dependents

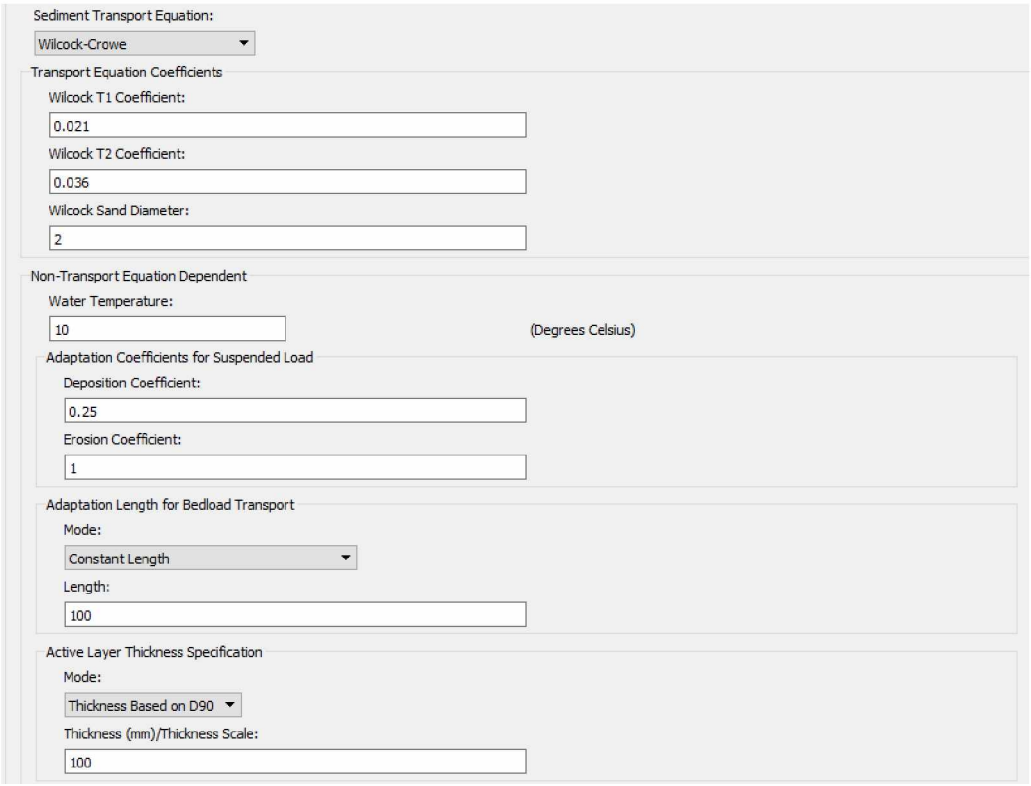

Figure C.2: Transport equation coefficients for the W-C equation and non-transport equation dependents

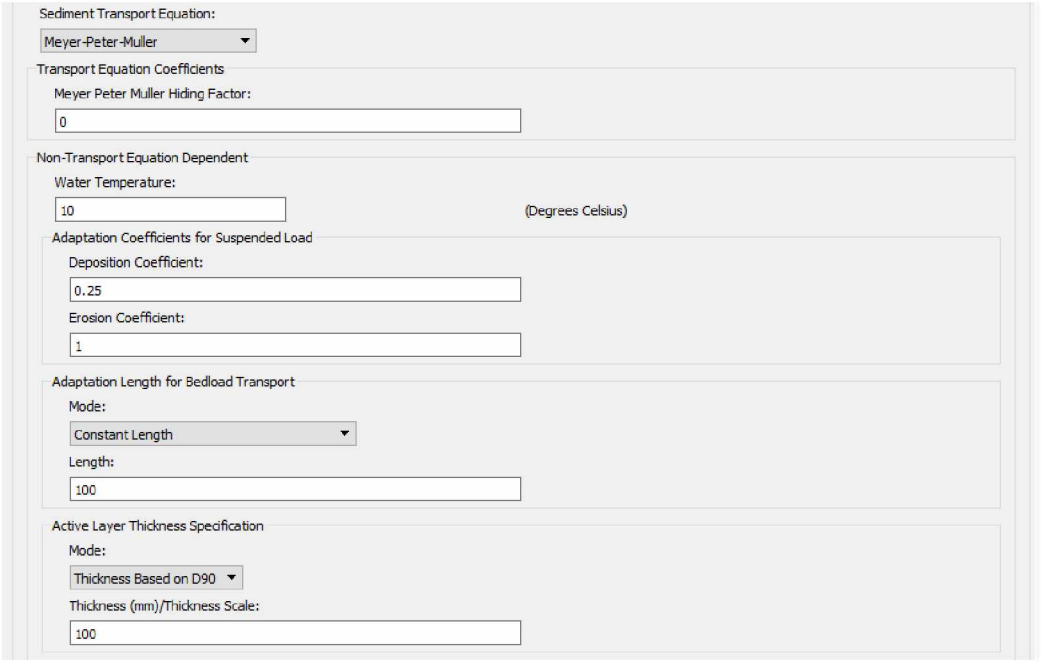

Figure C.3:Transport equation coefficients for the MPM equation and non-transport equation dependents

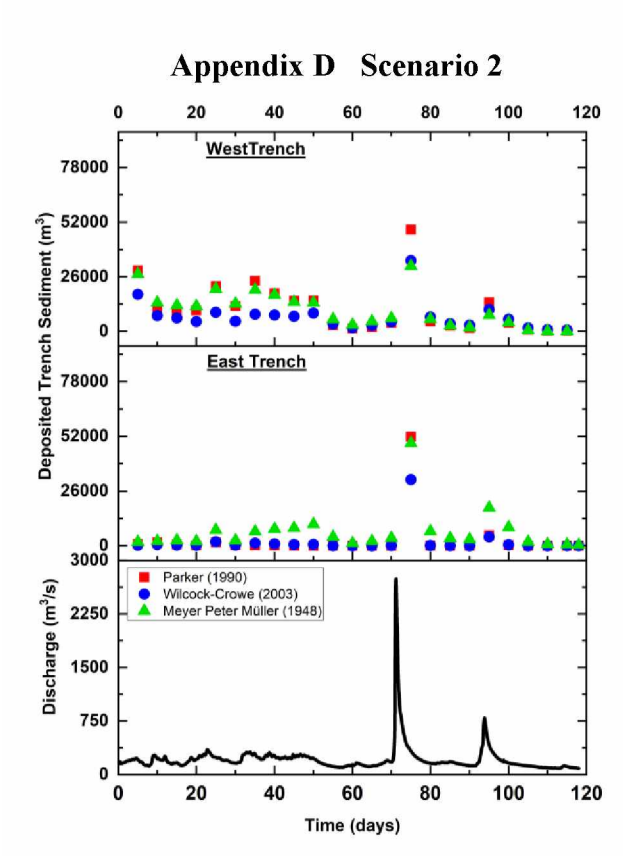

Figure D.1: Deposited trench sediment in m^3 for east and west trench as compared to the scenario 2 hydrograph

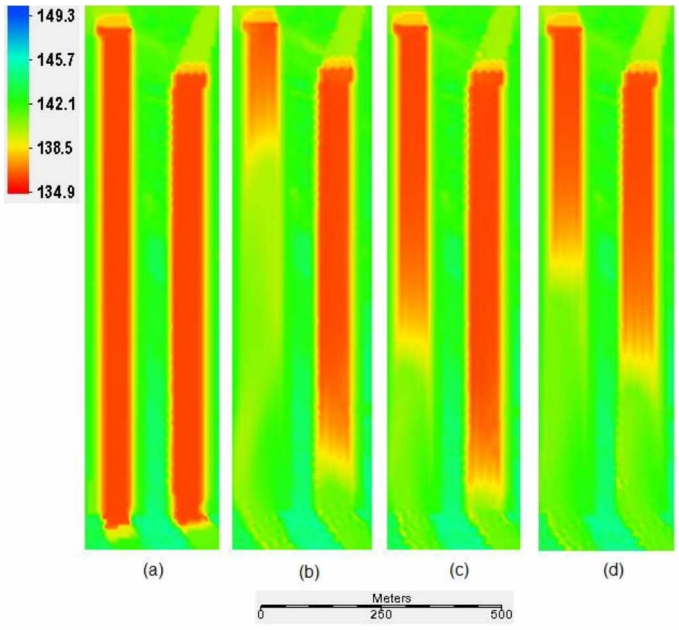

Figure D.2:Comparison of bed elevation in meters. Far left, (a) is the initial elevation. The three figures right show the simulation end for (b) Parker Eq. (c) W-C Eq. and (d) MPM Eq.

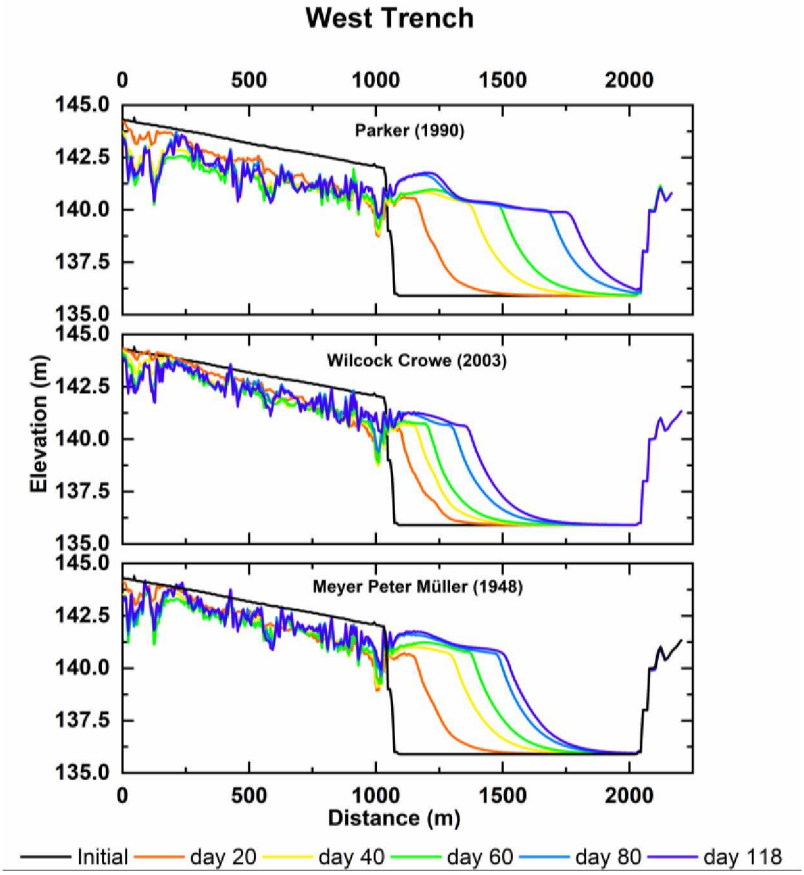

Figure D.3: Time series of west trench comparing bed elevation for each sediment transport equation during scenario 2

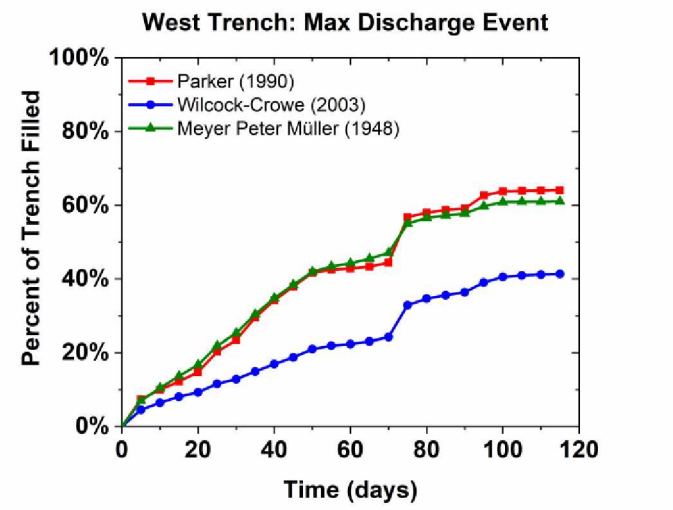

Figure D.4: Percent of west trench filled during scenario 2

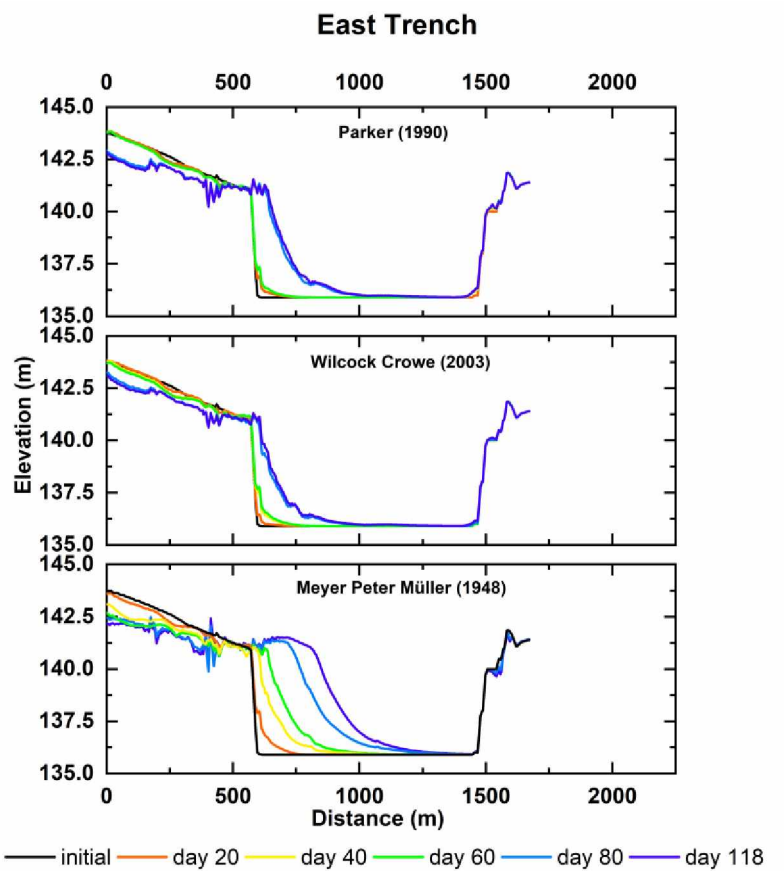

Figure D.5: Time series of east trench comparing bed elevation for each sediment transport equation during scenario 2

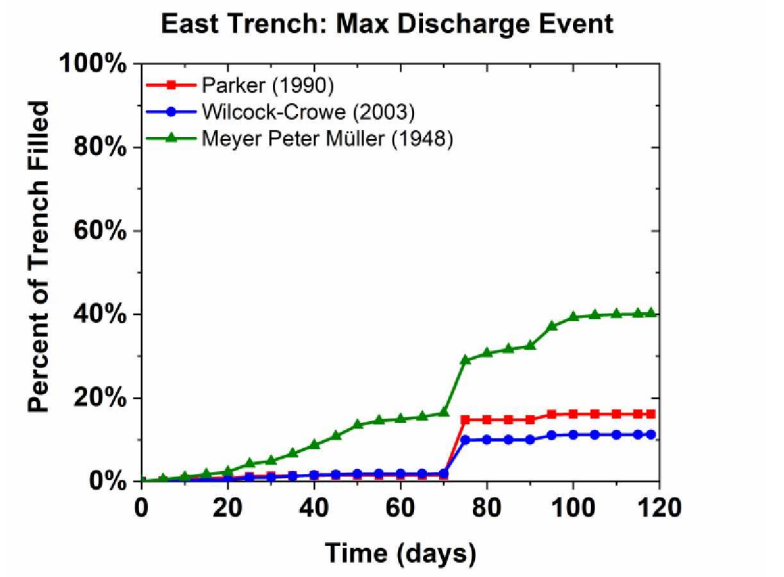

Figure D.6: Percent of east trench filled during scenario 2

Appendix E Scenario 3

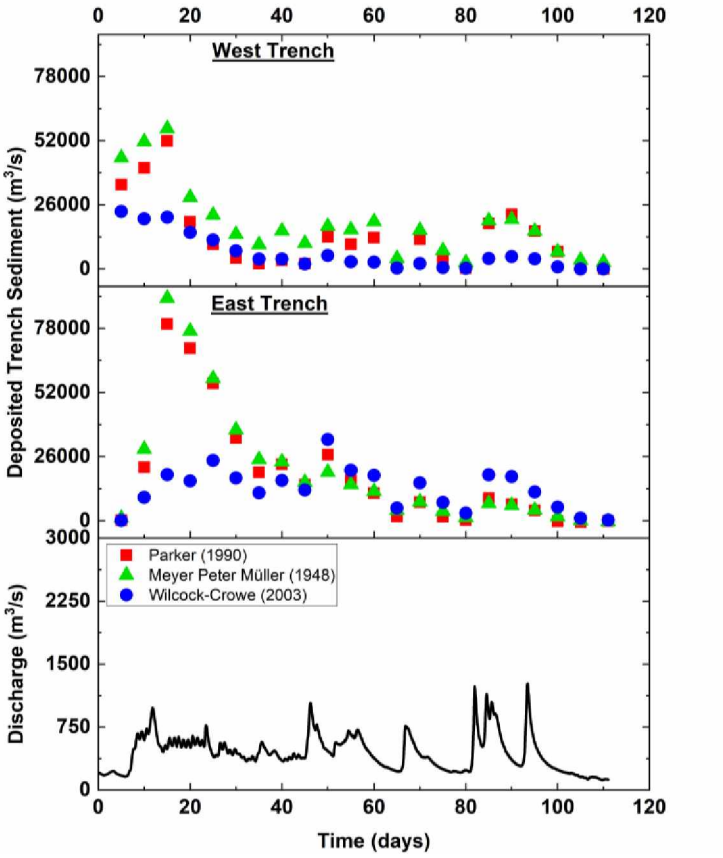

Figure E.1:Deposited trench sediment in m3 for east and west trench as compared to the scenario 3 hydrograph

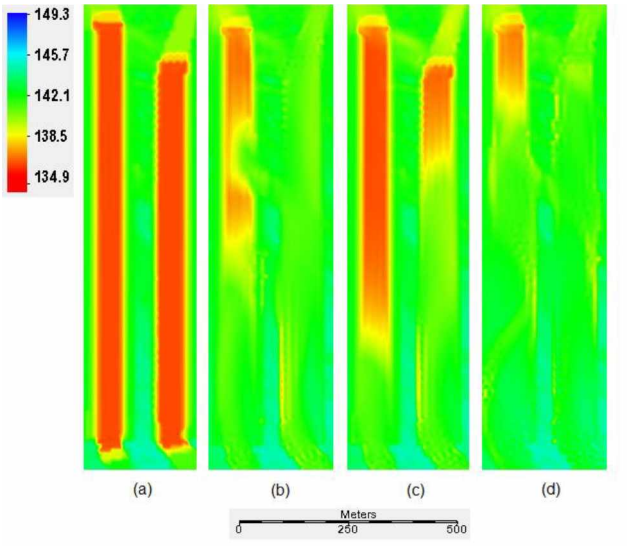

Figure E.2: Comparison of bed elevation in meters. Far left, (a) is the initial elevation. The three figures right show the simulation end for (b) Parker Eq. (c) W-C Eq. and (d) MPM Eq.

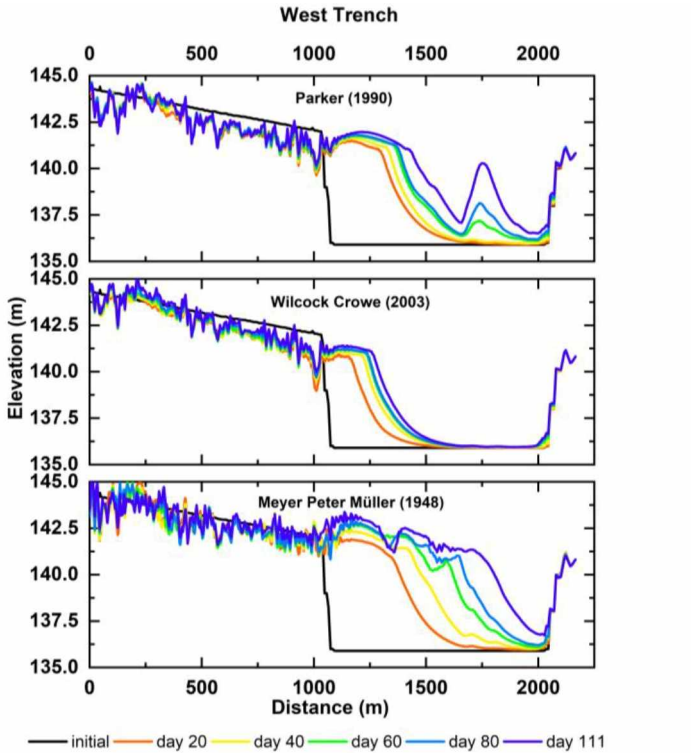

Figure E.3: Time series of west trench comparing bed elevation for each sediment transport equation during scenario 3

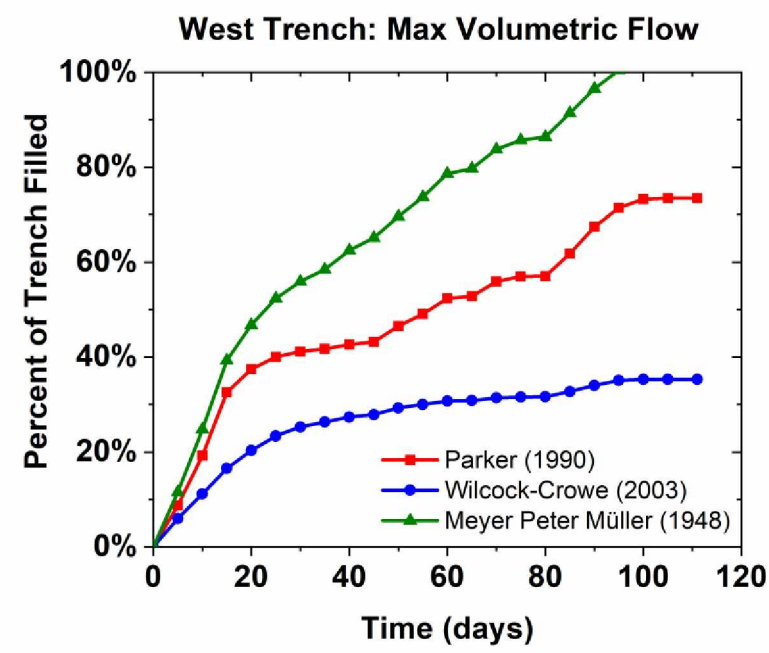

Figure E.4: Percent of east trench filled during scenario 3

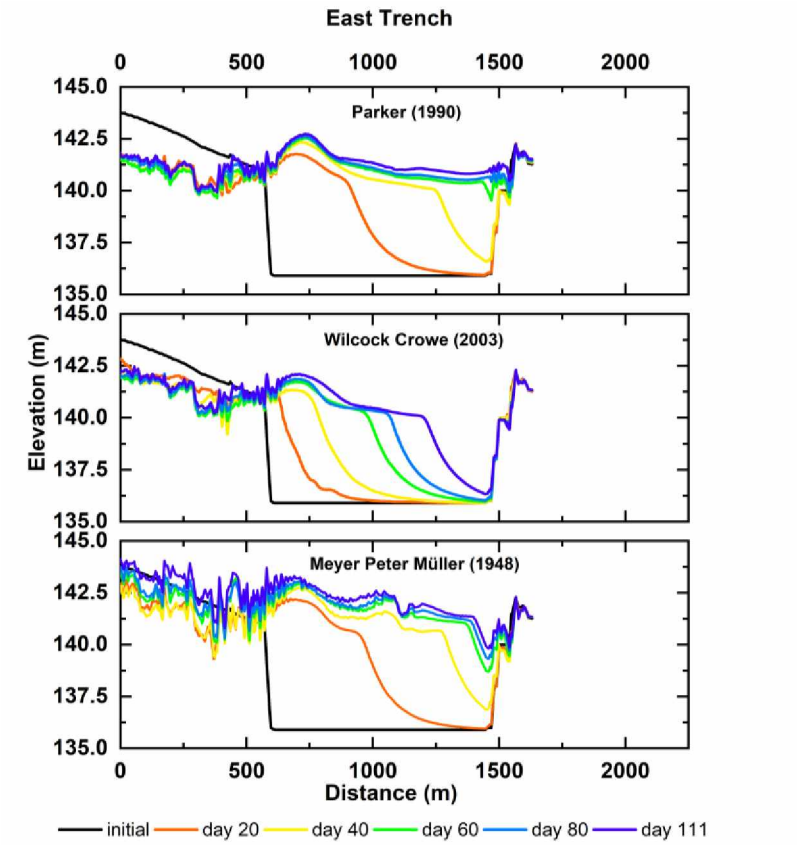

Figure E.5: Time series of east trench comparing bed elevation for each sediment transport equation during scenario 3

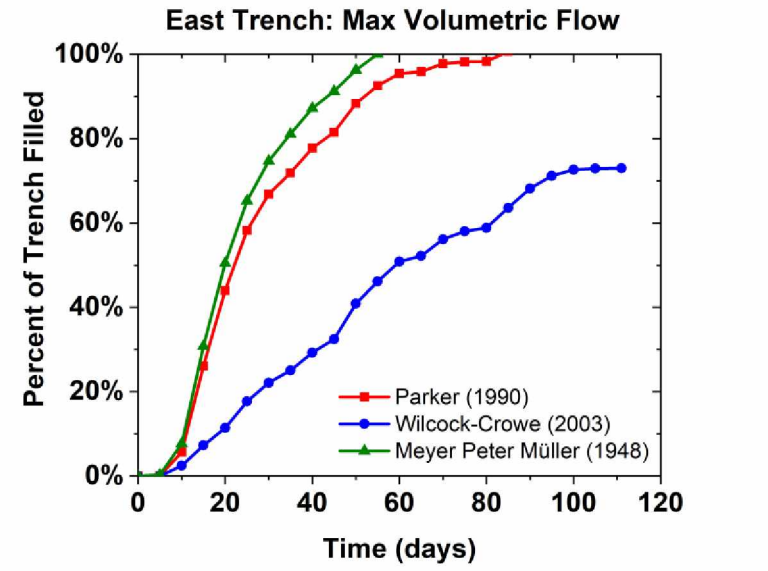

Figure E.6: Percent of east trench filled during scenario 3